University of Natural Resources and Life Sciences,
Vienna
Department of Biotechnology

Master Thesis

Establishing a RAW 264.7 cell culture model to study the effects of miRNAs on osteoclast differentiation

submitted by
Viktoria Wiedemann, B.Sc.

Supervisors:

Assoc. Prof. Dr. Johannes Grillari
Dipl. Ing. Dr. Matthias Hackl

1 Contents

2 Abstract

During the last years, many publications summarised the important regulatory roles of microRNAs (miRNAs) in bone metabolism and their association to bone-related diseases. MiRNAs were shown to control the differentiation of osteoblasts and osteoclasts, two key players in the life-long process of bone remodeling. Furthermore these cells were demonstrated to communicate via the secretion of miRNA-containing vesicles, which generally enables the detection of miRNAs in body fluids, referred to as „circulating miRNAs". Such levels of circulating miRNAs were observed to change after the occurrence of osteoporotic fractures and recently, it was announced that due to certain miRNA signatures discrimination between osteoporotic patients and healthy persons was possible. These data led to the development of the worldwide first miRNA-based diagnostic test for early diagnosis of osteoporosis, which will undergo clinical validation until 2018. In order to understand the effects of prominent miRNAs on the underlying mechanism of disease, an in bone research generally accepted *In Vitro* osteoclast model was established, within the framework of this master thesis.

3 Kurzfassung

In den letzten Jahren haben viele Publikationen die bedeutende regulatorische Rolle von mikroRNAs (miRNAs) auf den Knochenmetabolismus und ihren Zusammenhang mit Erkrankungen des Knochenapparates beschrieben. Es wurde nachgewiesen, dass miRNAs die Differenzierung von Osteoblasten und Osteoklasten kontrollieren, zwei wesentliche Zelltypen im Knochenumbau, der lebenslang stattfindet. Weiters wurde erkannt, dass diese Zellen über die Sekretion von Vesikeln die miRNAs enthalten, miteinander kommunizieren. Dieser Prozess ermöglicht die Detektion von miRNAs in Körperflüssigkeiten wie Blutserum, wo sie als „zirkulierende miRNAs–bezeichnet werden. Die Konzentration von zirkulierenden miRNAs verändert sich nachweislich mit dem Auftreten von osteoporotischen Frakturen und erst kürzlich wurde gezeigt, dass aufgrund bestimmter miRNA-Signaturen zwischen Osteoporose-Patienten und gesunden Personen unterschieden werden kann. Diese Daten führten zu der Entwicklung des weltweit ersten miRNA-basierenden Diagnosetests für die frühzeitigere Erkennung von Osteoporose, welcher bis 2018 einer klinischen Prüfung unterzogen werden soll. Um die Auswirkungen dieser neuartigen miRNA Biomarker auf den grundlegenden Mechanismus der Erkrankung besser verstehen zu können, wurde im Rahmen dieser Masterarbeit ein in der Knochenforschung generell anerkanntes *In Vitro* Osteoklasten-Modell etabliert.

4 Introduction

Around the world, about 200 million people are estimated to suffer from osteoporosis [1] and in the coming decades the number of patients is expected to rise due to a global increase in humans´ life expectancy [2]. The following chapters provide background information on bone biology and discuss if miRNAs can be useful biomarkers for the clinical diagnosis and fracture risk prediction of osteoporosis in the future. With regard to this master thesis the role of miRNAs in osteoclast differentiation will be explained.

4.1 Bone biology

4.1.1 Bone structure and composition

Bone is the major building block of the human skeleton [3] and a specialised type of connective tissue [4]. Besides the mechanical supportive function and the protection of inner organs, bone plays an important role in the regulation of mineral homeostasis serving as a large storage reservoir for inorganic ions such as calcium and phosphate. In addition, bone is relevant to an intact immune system, since bone marrow is the site of haematopoiesis [3].

Bone is composed of an organic and an inorganic matrix. The **organic matrix** mainly consists of type I collagen (about 95 %) but also contains various non-collagenous proteins, proteoglycans, lipids and cells [3, 5]. The **inorganic matrix** is predominantly made by impure crystals of hydroxyapatite ($Ca_{10}(PO_4)_6(OH)_2$), which are deposited into the organic matrix, but to some extent also includes water [3, 5]. Because of this structural arrangement the skeleton becomes rigid and strong while still maintaining the necessary degree of elasticity to resist mechanical loading [3, 5].

With regard to porosity two types of bone, which are related to different functions, can be distinguished: cortical and trabecular bone. While **cortical bone** is highly dense providing the supportive and protective function, **trabecular bone** reduces the skeletal weight due to its meshwork structure and has a major metabolic function [3, 5].

4.1.2 Bone cells and the process of bone remodeling

Bone might be considered as an inert and static material that once formed, does not undergo changes anymore. But in fact, bone is a complex, living tissue that gets continuously remodeled throughout lifetime [3, 6]. The term **“bone remodeling”** describes thereby the coupled process of bone resorption and bone formation by two different types of specialised bone cells, called osteoclasts and osteoblasts [3, 5]. In the following, the most important bone cells are explained and illustrated in Figure 1:

Osteoblasts originate from the mesenchymal stem cell (MSC) linage and are responsible for the synthesis of bone matrix by secretion of type I collagen and non-collagenous proteins such as osteocalcin and osteopontin [3, 4]. Since osteoblasts are main producers of the Receptor Activator of Nuclear Factor κ B Ligand (RANKL), the most essential osteoclast differentiation factor, as well as its decoy receptor osteoprotegerin, they are important regulators of osteoclastogenesis [3]. When osteoblasts get embedded into bone matrix their morphology changes drastically and they start to differentiate towards **osteocytes** [7]. These star-shaped cells are the most abundant cell type in the skeleton and function as sensors, communicators and initiators of bone repair [7, 8]. Inactive bone surfaces that do not undergo any structural changes are covered by morphologically flat and elongated **bone lining cells** which also derive from the osteoblast lineage [5]. While MSCs differentiate into various cell types including osteoblasts, chondrocytes, adipocytes and myoblasts [3, 9], interestingly, bone-resorbing **osteoclasts** are of hematopoietic stem cell (HSC) origin and therefore related to immune cells [10]. Since this work focused on osteoclast differentiation chapter 4.1.3 devotes a separate section to this type of cell.

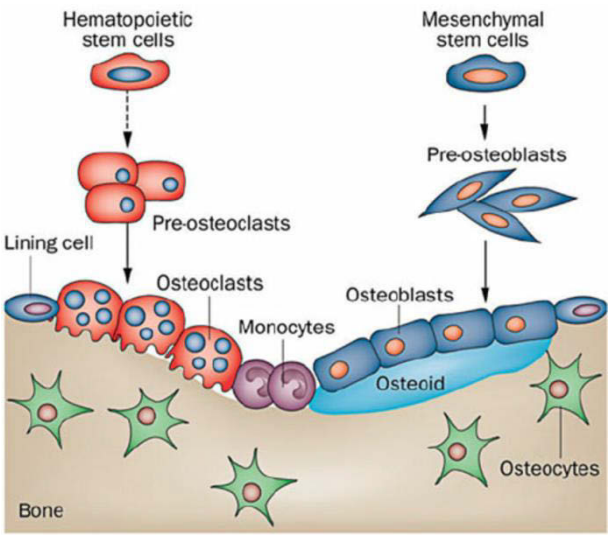

Figure 1: Bone cells.
While bone-forming **osteoblasts** are of mesenchymal origin, bone-resorbing **osteoclasts** derive from hematopoietic stem cells. Star-shaped **osteocytes** are the most abundant bone cell type and function as mechanosensors while bone **lining cells** cover inactive bone surfaces. Osteocytes and bone lining cells belong to the osteoblast linage. [© Lian et al 2012]

According to the study of Parfitt et al. [11] the process of **"bone remodeling"** can be divided into several phases: ***(I) activation, (II) bone resorption, (III) reversal, (IV) bone formation and mineralisation***, which last over several weeks [3]. ***(I)*** The cycle starts with the activation of a quiescent bone surface and the retraction of bone lining cells due to the influence of hormones (estrogen), drugs (corticosteroids) and/or importantly, osteocyte signalling [3]. ***(II)*** When the bone surface is uncovered, mononuclear osteoclast precursor cells get attracted and develop into mature, bone resorbing osteoclasts by the process of cell-cell fusion [3, 12]. ***(III)*** During a phase called reversal, the surface gets prepared for osteoblasts. ***(IV)*** Osteoblasts form the new bone matrix called ~~"o~~steoid" which needs to be mineralised afterwards [3, 13]. The cycle is finished when bone lining cells cover the surface. While bone resorption lasts for about 2 to 3 weeks, the synthesis of new bone matrix takes more time, usually 2 to 3 months [3]. Importantly, in terms of physiological bone remodeling, bone mass

and quality must always be kept constant [13, 14]. An imbalance in bone formation and bone resorption causes metabolic bone disorders such as osteoporosis [13, 14].

4.1.3 The osteoclast: a multinucleated, bone-resorbing cell

Osteoclasts are giant, multinucleated cells which derive from the monocyte/macrophage linage [3]. Since they are unique bone-resorbing cells they are essential players of bone metabolism [3]. The development of osteoclasts from their precursor cells is mediated by cell-cell fusion and requires two important factors: RANKL (receptor activator of NF-κB ligand) and MCS-F (macrophage colony stimulating factor) [3, 14]. While MCS-F promotes proliferation and survival of precursor cells, RANKL is known as the key differentiation factor of osteoclastogenesis since binding to its target receptor RANK, induces osteoclast differentiation [3, 14]. Mice lacking RANKL or RANK were not able to develop osteoclasts, resulting in a pathological condition called osteopetrosis, which is characterised by a decreased bone resorption [14]. As mentioned before, RANKL, as well as its soluble decoy receptor osteoprotegerin, are expressed on the surface of osteoblasts, which adds to the tight relationship of these two cell types in the process of bone remodeling [10, 14]. However, RANKL expression was also shown in osteocytes. [14] The regulation of osteoclastogenesis is depicted in Figure 2.

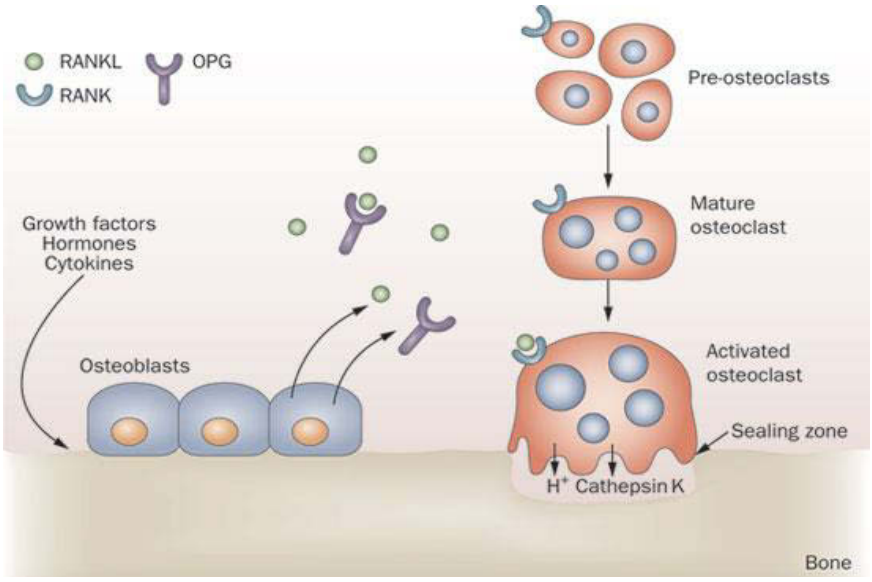

Figure 2: Regulation of osteoclastogenesis.
The RANKL/RANK/OPG system is essential for osteoclast maturation and inhibition. Upon RANKL binding to RANK receptor, which is expressed on osteoclast precursor cells, essential osteoclast genes get activated. Osteoprotegerin (OPG) is a decoy receptor of RANKL and can thereby inhibit the generation of osteoclasts. Both, RANKL and OPG are produced by osteoblasts. [©Lewiecky et al 2011]

The RANK-signalling cascade is initiated upon RANKL binding [3, 14]. It acts through TNF receptor associated factor 6 (TRAF6) and activates six important signalling pathways: NF-κB, JNK, ERK, p38, Akt and NFATc1, which is considered the master regulator of osteoclastogenesis [14]. While the **RANKL/RANK/OPG system** is fundamental in the local

regulation of bone remodeling, bone homeostasis is also controlled by various hormones such as estrogen, parathyroid hormone (PTH), 1.25-dihydroxyvitamin D_3 as well as cytokines and chemokines. [3]

During osteoclast maturation the cell experiences big structural modifications, preparing it for the highly energy-demanding process of bone resorption [15, 16, 17]. The main changes include circular rearrangements of the actin cytoskeleton (**"Actin ring"),** the generation of the so called **"Sealing zone"** which tightly attaches the osteoclast to bone matrix via integrins and the conversion of the bone-facing, strongly folded membrane which is named **"Ruffled border"** [3, 14, 15, 17]. The tight attachment of the osteoclast to the bone matrix creates an isolated, acidic microenvironment (**Howship´s lacuna**/ **Resorption lacuna**), which is the site of bone dissolution [3, 14, 17]. This resorption pit is acidified through fusion events of acidic vesicles and by the use of a proton pump (vacuolar H^+-ATPase) coupled to a chloride channel [14, 15, 17]. Besides protons, bone degrading enzymes such as

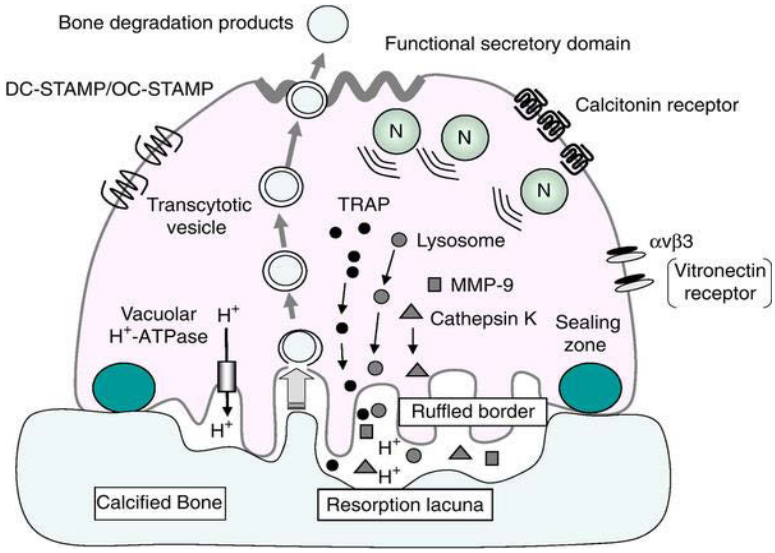

Figure 3: Structure and function of the mature, multinucleated osteoclast.
Mature osteoclasts contain specialised structural domains: The "Sealing zone" enables tightly attachment to the underlying bone matrix, thereby generating an acidic microenvironment called "Resorption lacuna". The proton pump (vacuolar H^+-ATPase) sits in the strongly folded membrane called "Ruffled border". Bone-destroying enzymes such as Cathepsin K and TRAP are introduced into the "Resorption lacuna". Bone degradation products are removed by transcytosis and released via the "Functional secretory domain". Mature osteoclasts express several surface receptors (e.g. calcitonin) and fusion molecules (DC-STAMP, OC-STAMP). [©Takahashi et al 2014]

Cathepsin K (Ctsk) and the tartrate-resistant acid phosphatase (TRAP) are transported through the ~~"~~Ruffled border" [12, 15, 17]. While osteoclast precursor cells express RANK and c-fms receptors for the recognition of RANKL and M-CSF, mature osteoclasts express calcitonin receptors as well as important fusion molecules like DC-and OC-STAMP [17]. Bone degradation products are removed by the process of transcytosis and released via a

“Functional secretory domain”, located on top of the cell [17]. The structural domains and functional molecules of osteoclasts that have just been described are illustrated in Figure 3.

4.2 Osteoporosis

Osteoporosis is a musculoskeletal disease characterised by a systemic reduction of bone strength and leads to an increased risk of bone fractures, especially in elderly people [18]. Bone strength is not only defined by bone density but also bone quality parameters such as architecture, mineralisation and the extent of microfractures [18]. Literally translated the term osteoporosis means **“porous bone”** [18].

In osteoporosis patients fragility fractures usually arise due to low-impact trauma such as falling from standing height [19]. Over the course of lifetime 15 to 30 % of men and 30 to 50 % of women are affected by osteoporotic fractures, indicating that women are at higher risk than men [19]. In Europe alone, 22 million females and 5.5 million males suffered from osteoporosis in the year 2010, with an increasing tendency, causing a high financial burden on public health care systems [20]. Since bone loss happens progressively but painless, patients are mostly not diagnosed until the occurrence of harmful fragility fractures [21, 22]. For that reason the disease has sometimes been called a ~~“s~~ilent killer” [21, 22]. The hip, wrist and spine are especially prone to break and cause patients to suffer from severe pain, limited mobility and loss of autonomy, associated with an increased risk of mortality [19].

In general, there is a classification into **primary and secondary osteoporosis** whereby primary osteoporosis is further subdivided into type I and II while secondary osteoporosis is linked to other diseases or treatment interventions such a corticoid therapy [13]. Type I (postmenopausal osteoporosis) is a common disease of postmenopausal women and arises due to estrogen deficiency, while type II (age-related osteoporosis) is linked to the aging process itself, affecting both women as well as men [13]. Still, bone loss can also occur in premenopausal women and young men [23].

According to the WHO criteria, measurement of the bone mineral density (BMD) by dual energy-X-ray absorptiometry (DXA) is recommended for the detection of osteoporosis [24]. However this technique has some limitations such as availability and high costs [24]. In addition BMD analysis alone might not be sufficient in the prediction of individual fracture risk [24] as more than half of the women that fracture do not have osteoporosis according to the bone mineral density criteria, although actually suffering from osteoporosis [25]. Therefore reliable biomarkers for an earlier diagnosis and fracture risk prediction are needed. MicroRNAs are a promising option [23].

Today, there are several therapeutic strategies to reduce the risk of bone fractures. Hereafter, only three major medications are listed. The most common administered drugs are

bisphosphonates which function through downregulation of osteoclast activity and lifespan [3]. Since estrogen deficiency is a main cause of postmenopausal osteoporosis another option is hormone replacement therapy aiming at the substitution of the absent hormone [3]. A prominent monoclonal antibody in the treatment of osteoporosis is called Denosumab and mimics the effect of osteoprotegerin by directly targeting RANKL [3].

4.3 MicroRNAs

MicroRNAs (miRNAs) are small, non-coding RNAs which serve as important post-transcriptional regulators of gene expression and remained highly conserved during evolution [26, 27].

4.3.1 Discovery

The first miRNA was identified during developmental studies combined to genetic screens in the nematode *Caenorhabditis elegans* in 1993 [27]. While protein encoding genes were already known at that time, *lin-4* was something special, since this gene encoded for a small RNA, which was shown to negatively regulate the worm developmental protein lin-14 [28].

4.3.2 Biogenesis and function

The biogenesis pathway of miRNAs includes several steps (see Figure 4) and starts with the generation of primary transcripts (pri-miRNA) from gene transcription ***(I miRNA gene transcription)*** [29]. Pri-miRNAs contain a hairpin structure and can be thousands of nucleotides long [29]. In the nucleus such primary transcripts get cleaved into stem-loop containing pre-miRNAs (~ 70 nt) by an enzyme called Drosha which is known to form a complex with the DGCR8 protein ***(II pri-miRNA cleavage)*** [26, 29, 30]. Following nuclear processing the pre-miRNAs are transported to the cytoplasm by Exportin 5, a Ran-GTP-dependent transporter ***(III export to cytoplasm)*** [30]. Inside the cytoplasm, the loop structure is cleaved off by Dicer ***(IV pre-miR cleavage)***, yielding short miRNA duplexes

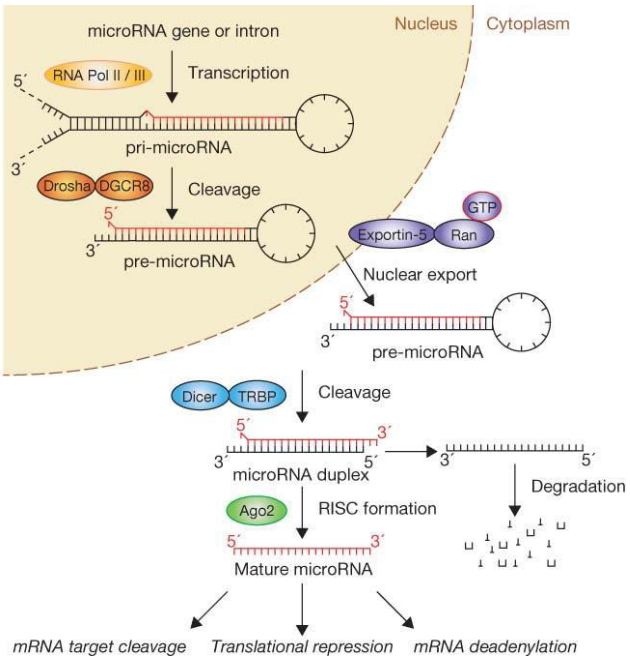

Figure 4: Biogenesis of miRNAs.
(I) After miRNA gene transcription, **(II)** pri-miRNAs get cleaved into pre-miRs by the Drosha-DGCR8 complex and are **(III)** exported to the cytoplasm by the Ran-GTP-dependent Exportin-5 transporter. **(IV)** The loop structure of the pre-miR is then cleaved off by the Dicer-TRBP complex resulting in a miRNA duplex. **(V)** In the RISC, usually, one strand gets selected to maturate while the other is often degraded. **(VI)** Mature miRNAs target mRNAs **(VII)** in order to inhibit the translational process. [©Winter et al 2009]

(~21 nt) which get incorporated into the RNA-inducing silencing complex (RISC), which besides Dicer includes TAR-RNA binding proteins (TRBP), protein activator of PKR (PACT) and argonaute protein (Ago) [29]. Drosha and Dicer are RNase III-type endonucleases and are key enzymes of miRNA maturation [29]. The miRNA duplex gets then separated into two single strands by the activity of a helicase and usually only one strand is selected as the mature, gene-regulating miRNA while the other strand is mostly degraded ***(V strand selection)*** [29]. Thermodynamic properties such as the stability of the 5´ends are believed to be crucial for strand selection [28]. Mature miRNAs are important post-transcriptional regulators of gene expression [29]. They function through binding to miRNA recognition sites, termed ~~-~~seed region", in the 3´UTR of target mRNAs ***(VI mRNA targeting)*** [29] which can lead to translational repression, mRNA degradation or mRNA deadenylation ***(VII translational inhibition)*** [31].

4.3.3 The role of miRNAs in osteoclast differentiation

MiRNAs have been proven as important regulators in the process of bone remodeling [32], since the complete loss of miRNA activity in osteoclast precursors resulted in the suppression of mature osteoclast formation [33]. In particular, the deletion of crucial proteins such as Dicer, DGCR8 and Ago2 involved in miRNA biogenesis in mononuclear osteoclast precursors resulted in a skeletal phenotype characterized by an increased bone mass due to a reduction in the number and activity of osteoclasts [33, 34, 35].

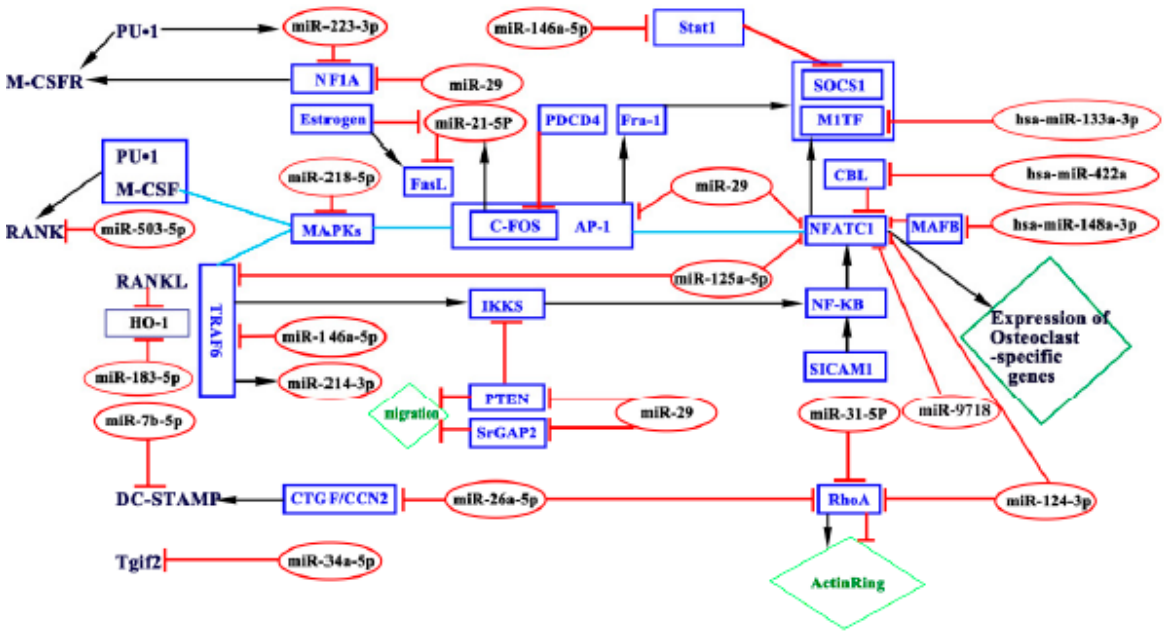

Figure 5: Target genes and effects of miRNAs on osteoclastogenesis.
MiRNAs (circled in red) target certain genes of the osteoclast differentiation pathway (marked in blue) such as RANK, TRAF6 or the key regulator NFATc1 in order to promote or inhibit osteoclastogenesis. Promoting miRNAs include: miR-21-5p, miR-29, miR-31-5p, miR-133a-3p, miR-422a, miR-148a-3p, miR-183-5p, miR-214-3p, miR-223-3p and miR-9718. Inhibiting miRNAs include: miR-7b-5p, miR-26a-5p, miR-34a-5p, miR-124-3p, miR-125a-5p, miR-146-5p, miR-218-5p, miR-503-5p. [©Ji et al 2016]

In addition miRNAs have been shown to be linked to bone diseases such as osteoporosis, osteoarthritis and rheumatoid arthritis [36]. Figure 5 presents the effects and target genes of already known bone-regulating miRNAs.

Osteoclastogenesis-promoting miRNAs include miR-21-5p and miR-148a-3p, which were both tested in this study. MiR-21-5p was shown to have high expression levels in osteoclast precursors which further increased during RANKL-induced osteoclastogenesis [37]. Furthermore, miR-21-5p synthesis is downregulated by the action of estrogen, a hormone known to inhibit osteoclastogenesis and to induce apoptosis of osteoclasts [38, 39]. Downregulation of miR-21-5p removes the inhibitory effect on FasL wherefore miR-21-5p cannot only promote osteoclastogenesis but also triggers apoptosis of osteoclasts [32]. Regarding miR-148a-3p, the analysis of miRNA expression profiles in CD14+ PBMCs, which were treated with MCS-F and RANKL, showed a clear upregulation of miR-148a-3p during osteoclastogenesis [40]. The effect of miR-148a-3p was further investigated in CD14+ PBMCs [41]. While an overexpression of this miRNA facilitated osteoclast formation, miRNA-inhibition suppressed it [40]. Other examples of promoting miRNAs include miR-29, miR-31-5p, miR-133a-3p, miR-422a, miR-183-5p, miR-214-3p, miR-223-3p and miR-9718 which were summarised in a review of Ji et al. [27].

Osteoclast-inhibiting miRNAs affect prominent targets such as the RANK receptor (miR-503-5p), the osteoclast master regulator NFATc1 (miR-214-3p) and DC-STAMP (miR-7b-5p), a key molecule of OC precursor cell fusion [27]. Figure 5 gives a schematic overview of important miRNAs including their target genes in the regulation of osteoclastogenesis.

4.3.4 Circulating miRNAs as biomarkers for osteoporosis

According to the WHO, a biomarker is defined as ~~a~~ny substance, its products, structure or process that can be measured in the body and that influences or predicts the incidence of outcome or disease" [41]. In the clinical diagnosis of osteoporosis dual-X ray absorptiometry (DXA) and the WHO-fracture risk assessment tool (FRAX®) are two recommended and validated methods of choice [41]. However, these tools still have some limitations, especially with regard to fracture risk prediction [41].

The role of **"circulating miRNAs"**, in form of miRNA-containing extracellular vesicles, was firstly recognised in the year 2007 and described a novel genetic exchange mechanism between cells [41]. By now, studies demonstrated that EVs are not secreted at random, but can be stably transported over long distances and delivered to acceptor cells (see Figure 6) [41]. In the context of bone biology, communication through EVs has been reported between osteoblasts and osteoclasts [42]. Importantly, several studies investigated the role of miRNAs in osteoporosis [42, 43, 44, 45]. For instance, the miRNA expression levels of

monocytes from high or low BMD postmenopausal women were compared and revealed an upregulation of miR-133a in the low BMD group [42]. In another study, osteoporotic against non-osteoporotic fracture patients were analysed in order to identify miRNA expression differences [43]. Here, five miRNAs (miR-21, miR-23a, miR-24, miR-25, miR-100, and miR-125b) were shown to be upregulated in the serum as well as bone tissue of the osteoporotic fracture patients [45]. Weilner et al., reported that ~~"~~circulating miRNAs" were changing in response to osteoporotic fractures and demonstrated that five of those differentially expressed miRNAs (let-7g-5p, miR-10b-5p, miR-100-5p, miR-148a-3p and miR-21-5p) could influence the osteogenic differentiation behaviour of mesenchymal stem cells [44]. Recently, it was published that serum miRNAs were indicative for fragility fractures in postmenopausal women with or without type 2 diabetes [45]. All these finding suggest that ~~"~~circulating miRNAs~~"~~could serve as biomarkers for a clinical diagnosis and fracture risk assessment in the future. However, this needs to be further investigated.

Figure 6: Schematic illustration of circulating miRNAs.
[© TAmiRNA GmbH]

4.4 RAW 264.7: an immortal, murine osteoclast precursor cell line

In the past, studying osteoclast function and development was limited to the isolation of mature cells from animal bone tissue [46, 47]. Later, osteoclast differentiation was induced by coculture systems of osteoblasts and osteoclast precursor cells [46, 47]. However the generation of pure osteoclast cultures was problematic until the discovery of RANKL, the key osteoclast differentiation stimulator [46, 47]. Today, many researches are able to generate osteoclasts simply by the addition of recombinant RANKL to primary bone marrow cells or peripheral blood mononuclear cells (PBMCs) [46, 47]. However, these procedures still require the isolation of the primary precursor population from their reservoir (see Figure 7), mostly from bone marrow and blood [46, 47]. While primary cells are limited in terms of availability, immortal cell lines such as RAW 264.7 are not [46, 47].

The murine, monocyte RAW 264.7 cell line provides an abundant source of osteoclast precursors [46, 47]. It was established in 1978 ~~"~~from the ascites of a tumor induced by a male mouse by intraperitoneal injection of Abelson leukemia virus" [46, 47]. RAW 264.7 cells have been used extensively in macrophage studies for more than 30 years [46, 47]. Moreover, RAW 264.7 cells can differentiate into osteoclasts since they are RANKL-

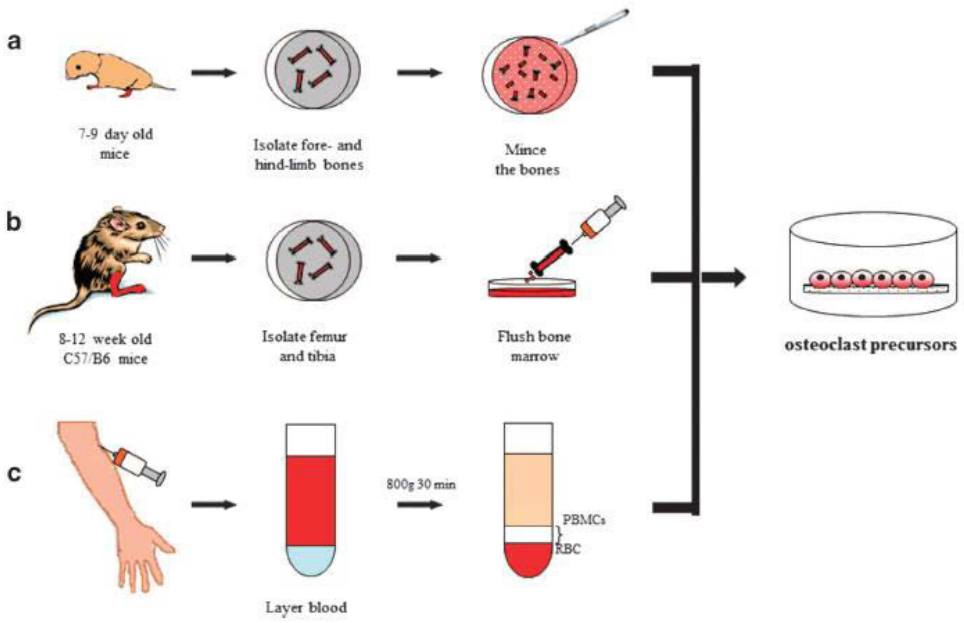

Figure 7: Sources of primary osteoclast precursor cells.
(a) Isolation from bone fragments of young mice **(b)** isolation from murine bone marrow **(c)** isolation from human blood [© Marino et al 2014]

responsive [46, 47]. In addition, these cells express both M-CSF and its associated receptor c-fms, wherefore it is not necessary to provide recombinant M-CSF during osteoclastogenesis [46, 47]. Furthermore mature osteoclasts from RAW 264.7 cells express hallmark characteristics as expected of fully differentiated osteoclasts from primary cells [46, 47]. Nevertheless it should be considered that immortal cells behave different in some ways than primary cells and should therefore only be used in preliminary studies or in combination with primary experiments [46, 47]. Anyway there are several advantages of using these cells instead of primary cells such as: (i) unlimited availability, (ii) reduced animal killing (iii) rather pure osteoclast cultures in comparison to coculture systems (iv) quickly osteoclast generation within days (v) large numbers of osteoclasts, (vi) expression of osteoclast hallmark characteristics, and (vii) relative easy transfection potential [46, 47].

5 Aim

During the last years, miRNAs have been identified as important regulators of bone metabolism. However, little is known about their detailed functions and target genes in osteoclast differentiation, when compared to osteogenesis. Therefore the aim of this work was the establishment of an *In Vitro* model from the immortal, murine RAW 264.7 cell line, to study the effects of certain miRNAs upon osteoclastogenesis. The key stones in establishing this *In Vitro* model are shown in Figure 8.

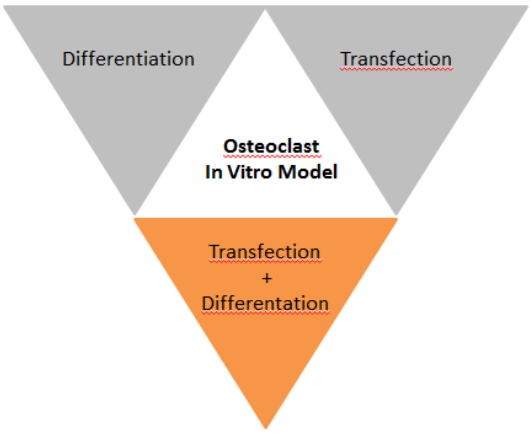

Figure 8: Scheme of working steps in the development of an osteoclast *In Vitro* model.
First, differentiation and transfection procedures had to be optimised until both methods could be combined to result in the osteoclast *In Vitro* model.

The ultimate goal of our research includes the evaluation of circulating miRNAs as novel biomarkers for age-associated diseases such as osteoporosis, cardiovascular and neurodegenerative diseases. Recently, it was published that certain miRNAs are strongly associated with the risk of bone fractures in postmenopausal women with and without type-2 diabetes [45], which suggests a great opportunity for these molecules to serve as diagnostic tools in the future.

6 Materials and Methods

6.1 Cell culture

6.1.1 Cell line and culture conditions

The murine monocyte/macrophage RAW 264.7 cell line was obtained from the American Type Culture Collection (ATCC® TIB71™; cell information: see Table 1 and Figure 9). For routine culture, RAW 264.7 cells were grown in 75 cm^2 flasks until 80 % confluence at 37 °C in a 7 % CO_2 humidified incubator. As suggested by the ATCC, cells were cultivated in DMEM high glucose (ATCC®; 30-2002) supplemented with 10 % FCS (Sigma-Aldrich®; F7524). Selection of the serum batch was done due to the results of preliminary experiments (data not shown). For the purpose of osteoclast differentiation cells were maintained in DMEM high glucose or α-MEM (Biochrom GmbH; F0915). With the addition of GlutaMAX™ Supplement (Gibco™; 35050061) a final L-glutamine concentration of 2 mM was set to α-MEM. Serum concentration remained 10 % and all experiments were done without the addition of antibiotics.

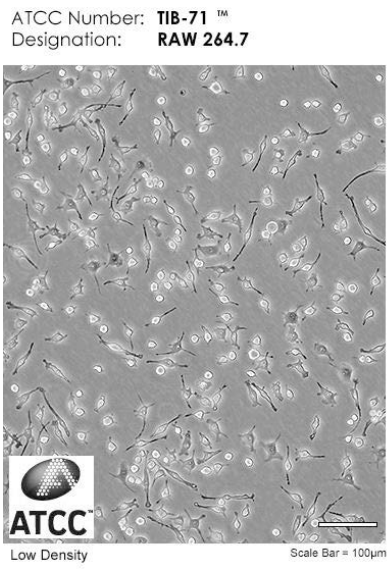

Figure 9: RAW 264.7 cell morphology in a low density culture from the ATCC® (TIB71™) [© ATCC]

Table 2 shows a comparison of selected DMEM-high glucose and α-MEM ingredients.

Table 1: RAW 264.7 cell line information

Cell line	RAW 264.7
Species	Mus musculus
Strain	BALB/c
Tissue origin	ascites (Abelson murine leukemia virus induced tumor)
Age	adult
Gender	male
Morphology	monocyte/macrophage
Growth property	adherent
Medium	DMEM high glucose, supplemented with 10 % FCS
Subculturing	1:3 to 1:6 (up to 1:10 in this study; when reaching 80 % confluence)
Medium renewal	every 2 to 3 days
Culture conditions	37 °C, 5 % CO_2 in air atmosphere (7 % CO_2 in this study)
Biosafety level	2

Table 2: Comparison of DMEM-high glucose and α-MEM composition

Cell culture medium	D-Glucose [mg/L]	L-Glutamine [mM]	Sodium bicarbonate [mg/L]
DMEM-high glucose	4,500	4	1,500
α-MEM	1,000	2	2,000

6.1.2 Passaging and harvesting

After some time, adherent cells such as RAW 264.7 start to cover the whole cultivation area. To provide the cells new space and to avoid nutrient depletion cells have to be subcultured regularly. Therefore the spent medium was aspirated and the cells were washed with 1x PBS twice to remove any dead cells. Carefully the washing solution was pipetted to the opposite site of the cell layer, the flask was gently moved several times and the PBS discarded. Fresh, prewarmed medium (at least RT) was then added and the cells were gently detached with the use of a cell scraper (SPL life sciences, 90030). Resuspension was achieved by pipetting up and down for two times.

To passage the cells a part of the cell suspension was transferred to a new 75 cm^2 culture flask (Greiner Bio-One, 658170) and filled up to 10 ml with prewarmed culture medium. Subculturing was done two to three times a week with split ratios from 1:4 to 1:10.

To harvest the cells for further experiments the cells were scraped into 10 ml of culture medium and the cell number was determined as described in 6.2.1. For most differentiation and transfection experiments one 75 cm^2 flask (80 % confluent) provided enough cell material.

6.1.3 Cryopreservation

Without the addition of cryo-protective agents, such as Dimethyl sulfoxide (DMSO), cells would be damaged by the formation of big ice crystals or due to osmotic cell lysis [48]. Nevertheless it has to be considered that DMSO-treatment has a toxic effect on cells at RT [48]. For that reason cell freezing and cell thawing processes had to be performed as quickly as possible.

For long-term storage cell vials were kept at – 80 °C. Cells were grown to 80 % confluence and 25 cm^2 of cultivation area were harvested per cryo tube. Freeze protection medium was made by the addition of 10 % DMSO (Sigma D2650) to the standard cell culture medium. To freeze cells of a 75 cm^2 flask, the medium was removed and the cells were washed with 1x PBS twice. Afterwards cells were scraped into 10 ml of culture medium and transferred into a 15 ml tube. After a centrifugation step (170 g; 5 min) the supernatant was carefully

aspirated and the cell pellet was loosened up by gently flicking the tube. Cells were resuspended in 3 ml of freeze protection medium and 1 ml of the suspension was filled in per cryo tube. Cell vials were immediately stored at -80 °C and transferred to the liquid nitrogen tank the following day.

6.1.4 Thawing of cells

To bring cells into culture one cell vial (per 75 cm^2 flask) was thawed in a 37 °C water bath. The anti-freeze medium had to be removed quickly since DMSO has a toxic effect on cells at RT. Therefore once the cells were thawed the suspension was immediately diluted in 5 ml of fresh culture medium using a 15 ml falcon tube. The cells were centrifuged at a moderate turn (170 g; 5 min) and the supernatant was carefully aspirated without disturbing the pellet. The cells were loosened up by gently flicking the tube, taken up in 10 ml of fresh culture medium and finally seeded into a 75 cm^2 flask. After 24 hours of incubation (37 °C; 7 % CO_2) the cells were checked under the microscope and the culture medium was exchanged.

6.1.5 Osteoclast differentiation

Since osteoclast differentiation protocols from RAW 264.7 cells vary a lot in terms of cell seeding density, culture medium, cultivation time and use of differentiation factors many conditions were tested until the generation of mature osteoclasts succeeded. It was recommended by Dr. Martina Rauner (Bone Lab Dresden) to use rather low population doublings (up to PD 25) since cells tend to loose differentiation capacity after some passages. Table 3 shows a list of tested differentiation factors with RANKL 462-TEC/CF reaching the best performance in this *In Vitro* model.

In the final differentiation protocol RAW 264.7 cells were maintained in α-MEM and seeded into 24-well plates (Greiner Cellstar®, 662160) at a density of 25,000 cells per 1.9 cm^2. To induce differentiation 20 ng/ml RANKL (R & D Systems; 462-TEC/CF) and 3.3 ng/ml TGF-β1 (R & D Systems; 7666-MB-005/CF) were added directly with seeding (day 0). On day 3 the medium was exchanged and on days 4, 5 (again medium exchange) and 6 osteoclast development was expected. Only TRAP (+), multinucleated (≥ 3 nuclei) cells were counted as osteoclasts.

Table 3: Differentiation factors for osteoclastogenesis

Differentiation factor	Final concentration [ng/ml]
RANKL (PeProTech 315-11; R & D Systems 462-TR/CF and 462-TEC/CF)	20 -100
TGF-β1 (R & D Systems; 7666-MB-005/CF)	3.3

6.1.6 Transfection of miRNA precursors

6.1.6.1 Electroporation using the Neon® Transfection System

Electroporation was done with the Neon® Transfection System (life technologies) according to the instruction manual. The electroporation parameters were adjusted as recommended for RAW 264.7 cells in the NEON™ cell protocol and are shown in Table 4. The volumes and concentrations of the transfection mixture are listed in Table 5.

Table 4: Electroporation parameters

Tip type [µl]	Pulse voltage [V]	Pulse width [ms]	Pulse number
10	1,680	20	1

At first culture plates were filled with medium and pre-warmed to 37°C. When using 6-well plates 2 ml of culture medium were used while with 25 cm^2 flasks 5 ml of medium were spent. Neon® tubes were filled with 3 ml of Buffer E and to avoid cross-contamination these tubes were always changed when switching to another nucleic acid template. Cells were harvested as described in 6.1.2 and the needed amount of cells was transferred into a 15 ml tube and centrifuged (170g; 5 min). The supernatant was carefully removed and the cell pellet was resuspended in 1 ml of 1x PBS. This suspension was transferred into a micro tube and centrifuged again (150g; 5 min). Meanwhile the pre-miRNA was pipetted to the bottom of a micro tube. 50 µM pre-miRNA aliquots (Thermo Scientific) were stored at -80°C until use and are listed in Table 8. After the centrifugation step 1x PBS was removed without touching the cell pellet and the cells were resuspended in Resuspension Buffer R. Now the cell suspension was added to already prepared pre-miRNA droplets and mixed by gently pipetting up and down. The Neon® Tip was attached to the Neon® Pipette and the cell-pre-miRNA suspension slowly sucked up avoiding the generation of any air bubbles which could lower transfection efficiency. When the pipette device was inserted into the Neon® Pipette Station the start button was pressed and cells were transfected by an electroporetic shock. Cells were quickly seeded into the prewarmed culture plate and placed into the incubator (37°C; 7 % CO_2) for 48 h.

Table 5: Transfection mixture used for electroporation

Tip type [µl]	Cell concentration [V]	Resuspension Buffer R [µL]	Pre-miR (10µM) [µl]
10	600,000	10	1

6.1.6.2 Lipid-based transfection using the siPORT™ NeoFX™ Transfection Agent

RAW 264.7 cells were transfected via the Reverse transfection procedure (see Figure 10) following the instructions of the user guide. In brief, lipids and miRNA precursor dilutions were mixed together allowing the formation of so called „transfection complexes". These transfection complexes tend to fuse with the cell membrane thereby delivering RNA cargo into the cell. For seeding the cells into 6-well plates Table 6 shows the composition and volumes of the transfection solutions. SiPORT™ NeoFX™ Transfection Agent (thermo fisher scientific AM4510) and Opti-MEM® medium (gibco 11058021) were prewarmed to RT and defined volumes of Opti-MEM® medium were put into micro tubes. RNA dilution and Lipid dilution were prepared by pipetting either pre-miRNA or siPORT™ NeoFX™ Transfection Agent to Opti-MEM® medium and mixed by gently pipetting up and down. RNA dilution and Lipid dilution were incubated for 10 min at RT. During that time cells were harvested and adjusted to an appropriate cell concentration of 2 * 10^5 cells/ 2.3 ml.

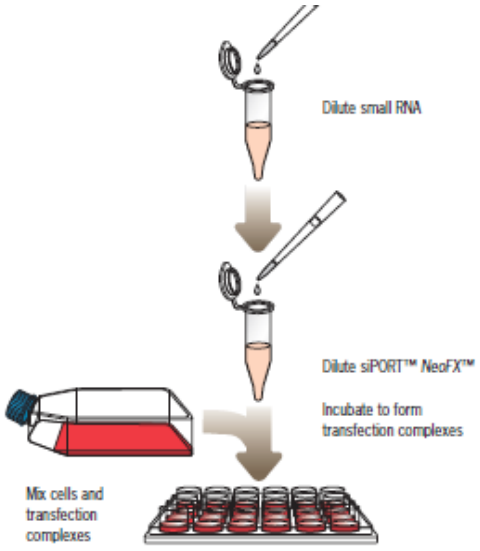

Figure 10: Scheme of reverse transfection procedure [© user guide; life technologies]

After 10 min of incubation 100 µl of RNA dilution were added to 100 µl of lipid dilution and gently mixed by pipetting up and down for three times. Now, another incubation step of 10 min at RT was necessary to allow the formation of the transfection complexes. Carefully this mixture was dropped into the well of the culture plate and overlaid by 2.3 ml of the cell dilution. An even distribution of the cells was obtained by moving the plate along an imagined infinite symbol. The cells were incubated (37 °C; 7 % CO_2) for 48 h until the day of analysis.

Table 6: siPORT™ NeoFX™ Transfection composition

Name	Reagent	Volume [µl]
Lipid dilution	siPORT™ NeoFX™ Transfection Agent	5
	Opti-MEM® medium	95
RNA dilution	pre-miRNA (10 µM)	7.5
	Opti-MEM® medium	92.5
Cell dilution	Cell overlay suspension	2,300
	Total cell number	2 * 10^5
Final volume		2,500

Estimation of the transfection efficiency was done by the introduction of Pre-miR Negative Control #1, FAM-labeled Pre-miR or Cy3-labeled Pre-miR from Ambion shown in Table 7. In contrast to the unconjugated Negative Control #1, the FAM™ and Cy3™-labeled Pre-miRs carry a fluorescence attachment which enables the detection of positively transfected cells by different technologies such as flow cytometry (see 6.2.2.1).

Table 7: Description of miRNA precursors used for the determination of transfection efficiency

miRNA precursor	Catalog #	Excitation max. [nm]	Emission max. [nm]
Pre-miR Negative Control #1	AM17110	-	-
FAM™-labeled Pre-miR	AM17121	494	520
Cy3™-labeled Pre-miR	AM17120	547	563

To test the impact of miRNAs upon osteoclast differentiation two already known differentiation enhancers, miR-21-5p and miR-148a-3p (listed in Table 8) were transfected into RAW 264.7 cells and 48 h later the differentiation was initiated as described in 6.1.5.

Table 8: Description of miRNA mimics used for RAW 264.7 transfection

miRNA	Catalog #	Conserved	Mature miRNA sequence
hsa-miR-21-5p	AM10206	yes (mmu-miR-21a-5p)	UAG CUU AUC AGA CUG AUG UUG A
hsa-miR-148a-3p	AM10263	yes	UCA GUG CAC UAC AGA ACU UUG U

6.2 Analytical methods

6.2.1 Cell count and viability analysis

Using the Vi-Cell XR Cell Viability Analyser (Beckman Coulter) allowed a fast and reproducible measurement of cell concentration and cell viability. The device is designed to count in the range of 50,000 to 10,000,000 cells per ml and it is possible to measure different cell types with a minimum size of 2 µm and a maximum size of 70 µm.

The principle of cell viability analysis is based on the Trypan Blue Dye Exclusion Method where dead cells appear in a blue colour while living cells remain unstained. The reason for this is that dead cells have a more permeable membrane than viable cells allowing the blue dye to enter the cell.

After cell detachment and resuspension 700 µl of cell suspension was pipetted reversely into a sample cap avoiding any air bubble formation which could falsify the results. The sample

was loaded by stating the right parameters such as cell type, sample position and sample ID before starting the measurement. The application provided results within a few minutes.

6.2.2 Passage Number vs. Population Doubling Level

As explained in the ATCC® Animal Cell Culture Guide the „Passage Number" corresponds to the number of times cells have been transferred into a new culture flask but gives no information on how often a cell has undergone cell division so far [49]. However this is of interest since every cell division causes telomere shortening, at least in primary cells [49]. Critically telomere shortening is known under the phenomenon of replicative senescence and makes cell division impossible [49]. This might not be relevant to an immortalised cell line like RAW 264.7 but as already mentioned these cells seem to change cell characteristics such as differentiation potential after some subculturing. Therefore it was decided to use the Population Doubling Level (see formula below) rather than the Passage Number. The „Population Doubling Level" (PDL) describes the total number of population doublings since cells were first isolated [49] and is calculated as follows:

$$N_t = N_0 * 2^{\frac{t}{t_D}}$$

$$\frac{N_t}{N_0} = 2^{\frac{t}{t_D}}$$

$$\log\left(\frac{N_t}{N_0}\right) = \frac{t}{t_D} * \log(2)$$

$$P_D = \frac{\log\left(\frac{N_t}{N_0}\right)}{\log(2)}$$

$$P_D = 3.32 * (\log(N_t) - \log(N_0))$$

$$P_{DL} = 3.32 * (\log(N_t) - \log(N_0)) + P_D$$

N	Final number of cells
N_0	Start number of cells
t	Cultivation time [h]
t_D	Doubling time [h]
P_D	Population doublings where PD = t/t_D
P_{DL}	Population Doubling Level

6.2.1 Population Doubling Time

The „Population Doubling Time" describes the time span a cell needs to duplicate [49] and was determined as shown in the formula below. Notably, the lag phase was not considered in the calculations.

$$t_{D=}\, t * \frac{\log(2)}{(\log(N_t) - \log(N_0))}$$

6.2.2 Determination of transfection efficiency

6.2.2.1 Flow cytometry

Flow cytometry provides information about cell number, size and morphology. Furthermore it can be used in the determination of transfection efficiency, distinguishing fluorescent from non-fluorescent cells. The principle is based on light-scattering where single cells pass through a laser beam and disperse the light in different angles. The so called „Forward Scatter" is proportional to the cell size while the „Side Scatter" gives information on cell granularity.

Table 9: Laser and Detectors used for FAM- and Cy3 detection

Laser	Detector
OPSL Sapphire 488 nm	FL1: 504 – 545 nm (FAM)
	FL2: 560 – 590 nm (Cy3)
	FL3: 603 – 699 nm (Cy3)

Cells were analysed 48 h after transfection using the Gallios Flow Cytometer (Beckman Coulter) according to the instruction manual. The culture medium was aspirated and cells were washed three times with 1x PBS to remove any unspecific fluorescence signal. Cells were scraped into 1 ml of 1x PBS, transferred into micro tubes and centrifuged (150 g; 5 min). Then the supernatant was carefully pipetted off, the pellet resuspended in 400 µl of 1x PBS and the suspension pipetted into flow cytometry tubes. Data analysis was done via the Kaluza Flow Cytometry Analysis Software.

6.2.2.2 Transfection assay

Another device for estimating transfection efficiency was the Luna-FL™ Dual Fluorescence Cell Counter. The advantages of this machine were the convenient handling as well as the low sample volume. Sample preparation was already described above and the following steps were done according to the Luna FL™ Quick Start Guide. In brief, 10 µl of sample (either control-transfected or fluorescence-transfected) were loaded into the chamber of a Photon Slide. As usual the negative control had to be set first providing information about the background fluorescence level. Table 10 includes relevant data from the specification list.

Table 10: Specifications of the Luna-FL™ Dual Fluorescence Cell Counter

Sample volume [µl]	Cell conc. [cells/ml]	Excitation [nm]	Emission [nm]
10	$5 * 10^4$ - $1 * 10^7$	470 ± 20	530 ± 25

6.2.3 Microscopy

RAW 264.7 cells were regularly checked under the microscope (Leica, Olympus) to study morphology and confluence. The magnifications ranged from 4 to 40 times. All pictures were made using Leica Application Suite (LAS), the platform of Leica microscopes.

6.2.4 Functional assays

6.2.4.1 TRAP staining

TRAP staining was done with the Acid Phosphatase Leucocyte (TRAP) Kit from Sigma Aldrich©. As described in the user manual the principle of this method is based on the formation of an insoluble, purple coloured diazonium salt. It results from a coupling reaction of diazotised Fast Garnet GBC Base Solution and dephosphorylated Naphthol AS-BI Phosphoric Acid Solution. Tartrate solution is added in order to inhibit other phosphatases than TRAP.

The cell culture medium was removed and the cells were fixed in 1 ml of OC Fixative Solution for 2–3 min at RT. The OC fixative solution was aspirated and the cells were washed three times with 1 ml of dH_2O. Solutions A and B were mixed immediately before usage and 1 ml of this mixture was added per well. When starting the master thesis the cells were now checked for colouring under the microscope and cells appeared violet after about 3 min. At this time point the substrate solution was removed and replaced by 1 ml of dH_2O. However, the incubation time had to be prolonged to 30 min (incubation in the dark) to enable the staining of large osteoclasts.

Table 11: TRAP staining solutions

Solution	Reagent	Volume [ml]
OC fixative solution	Acetone	6.5
	Citrate Solution	2.5
	36 % Formaldehyde	0.8
Solution A	Sodium Nitrite Solution	100
	Fast Garnet GBC Base Solution	100
Solution B	dH_2O	9,000
	Acetate Solution	400
	Tartrate Solution	200
	Naphthol AS-BI Phosphoric Acid Solution	100

6.2.4.2 TRAP assay

In order to obtain quantitative information on the enzymatic activity of TRAP the performance of a photometric assay was done.

First, all the materials and solutions were prepared and the pH of the 50 mM Citrate Buffer was checked regularly. The Buffer and the Substrate Solution were made freshly every time and the Substrate Solution was stored in the dark until use. Treatment of the cells started with aspiration of cell culture medium. The cells were fixed with 1 ml of 3,6 % Formaldehyde (10 min; RT) followed by another short fixation step with 1 ml of Ethanol/ Acetone solution (1 min; RT). After the addition of 200 µl Substrate Solution the cells were incubated in the dark for 1 hour. After incubation, 200 µl of Stop Solution (0.1 M NaOH) was added and a colour change from transparent to yellow indicated activity of TRAP. For further analysis 100 µl of the supernatant were transferred into a Nunclon 96 flat transparent plate (Thermo Fisher, 269620) performing three technical replicates. The samples were measured with a spectrophotometer at an absorbance value of 405 nm and a reference wavelength of 620 nm. Data are shown as mean values ± standard deviation (SD):

$$\bar{x} = \frac{x_1 + x_2 + \cdots + x_n}{n}$$

$$\sigma = \sqrt{\frac{\sum(x - \bar{x})^2}{n}}$$

σ	Standard deviation
∑	Summation
x	Value
x̄	Mean value
n	Number of values

Table 12: TRAP assay solutions

Solution	Reagent	Amount
Fixative solution	Formaldehyde (36 %)	1 ml
	dH_2O	9 ml
Fixative solution	Ethanol (100 %)	5 ml
	Acetone	5 ml
Citrate buffer (50 mM; pH=4.6)	Citrate buffer (0.1 M)	4 ml
	dH_2O	4 ml
Tartrate buffer	Citrate buffer (50 mM)	4 ml
	Sodium tartrate	9.2 mg
Substrate solution	Tartrate buffer	2 ml
	6 mM PNPP	4.44 mg
Stop solution	NaOH (0.1 M)	-

6.2.5 RNA analysis

Besides the functional assays, RNA analysis was fundamental for cell characterisation. On the one hand it was required to study the mRNA expression levels of certain osteoclast markers and on the other hand it was needed to check for overexpression of transfected miRNAs.

6.2.5.1 Cell lysis

Cell lysis was done with TRI reagent (Sigma T9424) in the hood. Therefore the culture medium was discarded and the cells were washed with 1 ml of 1x PBS to completely remove the residual medium. The 1x PBS solution was pipetted off and 0.5 ml of TRI reagent per 24-well was added. The culture surface was rinsed by pipetting up and down and the cell lysate was transferred to a micro tube. The samples were immediately stored at -80 °C until the isolation by a phenol/chloroform extraction.

6.2.5.2 Total RNA isolation

Total RNA isolation was done by phenol/chloroform extraction. All following steps were done in the hood and in order to avoid RNase contamination the working surface and lab equipment was cleaned with RNaseZAP® Wipes prior to isolation.

To purify total RNA from cell lysates the samples were thawed and 100 µl of Chloroform was added per 0.5 ml of TRI reagent. The samples were vortexed (15 s) and incubated at RT for 2–3 min. Separation of the organic and the aqueous phase was done by a centrifugation step (15 min; 12 000 g; 4 °C). The RNA-rich, upper phase was then transferred into a new micro tube avoiding to soak up proteins at the interface. Making the RNA pellet more visible 1 µl of GlycoBlue™ Coprecipitant was added and RNA precipitation was induced by the addition of 250 µl Isopropanol per 0.5 ml of TRI reagent. The samples were vortexed and incubated for 10 min at RT before another centrifugation step was done (10 min; 12 000 g; 4 °C) to settle RNA to the bottom of the tube. Carefully the supernatant was removed and the pellet was washed with 1 ml of 70 % Ethanol followed by a centrifugation step (5 min; 7 600 g; 4 °C). Again the supernatant was discarded and after a short centrifugation step (15–30 s; 7 600 g; 4 °C) the remaining liquid was removed as good as possible. With open lid the pellet was allowed to dry (no longer than 10 min) and resuspended in 20 µl NFW. Finally the samples were incubated at 58 °C for 10 min and stored at - 80 °C.

6.2.5.3 Nucleic acid concentration and purity control

To determine RNA or DNA concentration sample absorbance was measured at 260 nm using the NanoDrop™ One microvolume instrument (Thermo Scientific). As recommended in the user guide the purity of the samples was checked by the ratios of 260/280 and 260/230 nm. The former ratio is an indicator of protein and phenol contamination absorbing at 280 nm and should be in the range of 1.8 for DNA and 2.0 for RNA samples. The 260/230

ratio is an indicator of contaminants absorbing at 230 nm such as TRI reagent and should be in the range of 2.0 – 2.2.

6.2.5.4 cDNA synthesis

6.2.5.4.1 cDNA synthesis for mRNA expression analysis

The cDNA synthesis for quantitative real-time PCR (qPCR) analysis of mRNA expression levels was done using the Grand Script cDNA Synthesis Kit from Tataa (A103B) according to the manuals instruction. Briefly, all components were thawed on ice, gently vortexed (except the enzyme) and shortly centrifuged to collect liquid at the bottom of the tubes. RNA samples were diluted with NFW to a final amount of 500 ng per sample preparation. Components of Table 13 were pipetted into PCR tubes, gently mixed by flicking the tubes and shortly centrifuged to collect the content at the bottom. Samples were placed into the MasterCycler Nexus (Eppendorf) and cDNA synthesis was started with the conditions shown in Table 14.

Table 13: PCR composition for mRNA analysis

Reagent	Volume per sample preparation [µl]
TATAA GrandScript RT Reaction Mix (5x)	4.0
TATAA GrandScript RT Enzyme	1.0
RNA [500 ng total]	15.0
Final Volume	**20.0**

Table 14: PCR protocol for mRNA analysis

Step	Temperature [°C]	Time [min]
1: Activation	22	5
2: cDNA-strand synthesis	42	30
3: Inactivation	85	5
4: Hold	14	-

6.2.5.4.2 cDNA synthesis for miRNA expression analysis

The cDNA synthesis for quantitative real-time PCR of miRNA expression levels was done using the Universal cDNA synthesis kit II from Exiqon (203301). The PCR composition for miRNA analysis is listed in Table 15.

First, the RNA samples, NFW and 5x reaction buffer were gently thawed and then stored on ice during the whole work process. RNA samples were diluted with NFW to a final amount of

5 ng per one sample preparation. The enzyme was taken out of the fridge just before preparing the Master Mix and the 5x reaction buffer was mixed by vortexing. The reagents were spun down to collect all the liquid at the bottom and the Master Mix was prepared by pipetting all reagents except RNA into a micro tube. The liquid was homogenised by gently flicking the tube and shortly spinning down. Following 8 µl of the Master Mix was placed into PCR tubes and 2 µl of diluted RNA was added generating a total volume of 10 µl. The PCR tubes were shortly centrifuged and the PCR was started with the conditions shown in Table 16.

Table 15: PCR composition for miRNA analysis

Reagent	Volume per sample preparation [µl]
5x Reaction buffer	2.0
NFW	4.5
Enzyme	1.0
cDNA Spike-In	0.5
RNA [5 ng total]	2.0
Final Volume	**10.0**

Table 16: PCR Protocol for miRNA analysis

Step	Temperature [°C]	Time [min]
1: cDNA-strand synthesis	42	60
2: Inactivation	95	5
3: Hold	14	-

6.2.5.5 Quantitative real-time PCR

6.2.5.5.1 Quantitative real-time PCR for mRNA expression analysis

First the cDNA, primer pairs and Grandmaster Mix were thawed on ice. The cDNA was diluted 1:2 immediately before use and gently mixed by flipping the tube and a short spin down to collect the liquid on the bottom. The ingredients of the Master Mix (all reagents except cDNA template shown in Table 17) were put together and gently mixed. 8 µl of this Master Mix were pipetted into the wells of a 96-well plate and supplemented with 2 µl of the diluted cDNA. For the NTCs 2 µl of NFW were used instead of the cDNA template. The final volume was 10 µl per well. The plate was closed with a sealing foil and centrifuged (1 500 g; 90 s). Data analysis included comparison of Cq-values as well as melting curve analysis (see

Figure 29) to ensure product specificity. Osteoclast marker genes (e.g TRAP) were normalised to β-actin as a reference gene. All calculations were done to the following formulas (primer efficiencies listed in Table 25):

$$\Delta Cq_{undifferentiated} = Cq_{osteoclast\ marker\ gene} - Cq_{reference\ gene}$$

$$\Delta Cq_{differentiated} = Cq_{osteoclast\ marker\ gene} - Cq_{reference\ gene}$$

$$\Delta\Delta Cq_{undifferentiated} = \Delta Cq_{undifferentiated} - \Delta Cq_{undifferentiated}$$

$$\Delta\Delta Cq_{differentiated} = \Delta Cq_{differentiated} - \Delta Cq_{undifferentiated}$$

$$FC_{undifferentiated} = primer\ efficiency^{\Delta\Delta Cq_{undifferentiated}}$$

$$FC_{differentiated} = primer\ efficiency^{\Delta\Delta Cq_{differentiated}}$$

Table 17: Composition of the Master Mix for mRNA expression analysis

Reagent	Volume per sample preparation [µl]
Grandmaster Mix	5
Primer forward 1:100	0.4
Primer reverse 1:100	0.4
NFW	2.2
cDNA (1:2)	2
Final volume	**10**

Table 18: mRNA primer list

Gene	Product length [bp]	Sequence (5´→ 3´)
β-actin	89	Fw: GTC GAG TCG CGT CCA CC Rev: GTC ATC CAT GGC GAA CTG GT
TRAP	75	Fw: CGT CTC TGC ACA GAT TGC AT Rev: AAG CGC AAA CGG TAG TAA GG
Ctsk	75	Fw: AGC GAA CAG ATT CTC AAC AGC Rev: AGA CAG AGC AAA GCT CAC CAT
Atp6v0d2	89	Fw: AAG CCT TTG TTT GAC GCT GT Rev: GCC AGC ACA TTC ATC TGT ACC
OSCAR	377	Fw: GTC CTG TCG CTG ATA CTC CAG Rev: GGG AGC TGA TCC GTT ACC AG
CalcR	150	Fw: TGG TGC GGC GGG ATC CTA TAA GT Rev: AGC GTA GGC GTT GCT CGT CG

Table 19: Cycling Conditions for mRNA expression analysis

Step	Temperature [°C]	Time [s]	Number of Cycles
1: Pre-Denaturation	95	30	1
2: Denaturation	95	5	
3: Primer annealing	60	15	45
4: Elongation	72	10-30	
5: Melting Curve	95	10	
	55	60	1
	99	-	

6.2.5.5.2 Quantitative real-time PCR for miRNA expression analysis

For each different primer set (Exiqon) a Master Mix was prepared made up of the components listed in Table 20, except the cDNA template. Human primers (hsa) were sequence conserved except for miR-31. Therefore mmu-miR-31-5p was used. 6 µl of the Master Mix was placed into the well of a 96-well plate and supplemented with 4 µl of diluted cDNA (1:40). The plate was covered with a sealing foil and centrifuged (1,500g; 90s) to collect fluid at the bottom. The quantitative real-time PCR was performed using a Light Cycler 480 II (Roche) with cycling conditions set as shown in Table 22. The data was normalised to U6 and 5S as reference genes and related to the negative control. The following formulas provide an example calculation:

$$\Delta Cq_{neg.control-transfected} = Cq_{miR-X} - Cq_{reference\ gene}$$

$$\Delta Cq_{miR-transfected} = Cq_{miR-X} - Cq_{reference\ gene}$$

$$\Delta\Delta Cq_{neg.control-transfected} = \Delta Cq_{neg.control-transfected} - \Delta Cq_{neg.control-transfected}$$

$$\Delta\Delta Cq_{miR-transfected} = \Delta Cq_{miR-transfected} - \Delta Cq_{neg.control-transfected}$$

$$FC_{neg.control-transfected} = 2^{\Delta\Delta Cq_{neg.control-transfected}}$$

$$FC_{miR-transfected} = 2^{\Delta\Delta Cq_{miR-transfected}}$$

Table 20: composition for miRNA expression analysis

Reagents	Volume per sample preparation [µl]
PCR Master mix	5
PCR Primer mix	1
cDNA (1:40 dilution)	4
Final volume	**10**

Table 21: miRNA primer list

Name	Conserved	target sequence
5S rRNA		
U6 snRNA		
hsa-miR-21-5p	yes	UAG CUU AUC AGA CUG AUG UUG A
hsa-miR-148-3p	yes	UCA GUG CAC UAC AGA ACU UUG U
mmu-miR-31-5p	no	AGG CAA GAU GCU GGC AUA GCU G
hsa-miR-200b-3p	yes	UAA UAC UGC CUG GUA AUG AUG A
hsa-miR-29b-3p	yes	UAG CAC CAU UUG AAA UCA GUG UU
hsa-miR-188-3p	yes	CUC CCA CAU GCA GGG UUU GCA

Table 22: Cycling Conditions for miRNA expression analysis

Step	Temperature [°C]	Time [s]	Number of cycles
1: Activation	95	600	1
2: Amplification	95	10	45
	60	60	
3: Melting Curve	95	10	
	55	60	1
	99		

7 Results

7.1 RAW 264.7 characterisation

7.1.1 Morphology and growth characteristics

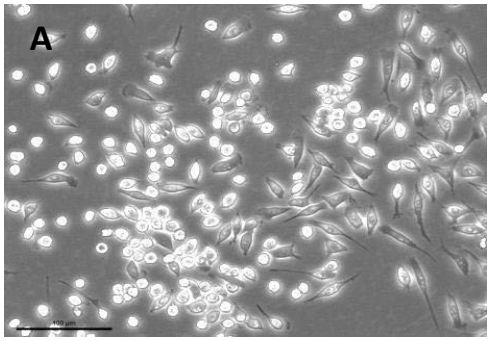

Figure 11: RAW 264.7 morphology (PD32).
Cells show typical monocyte/macrophage morphology with semi-adherent growth properties. The scale bar represents 100 µm.

RAW 264.7 cells (ATCC® TIB71™) grown in 75 cm^2 flasks showed the typical monocyte/macrophage morphology with semi-adherent growth properties. Cell proliferation was observed to be high wherefore cells were passaged two to three times per week at split ratios up to 1:10. A higher split ratio was not recommended since cells started to proliferate slower with a reduction in cell viability. At higher cell densities cells tended to detach leading to the formation of multi-layers.

7.1.2 Population doubling time of RAW 264.7 cells

To determine the population doubling time of RAW 264.7, a defined number of cells was seeded (1,000,000 cells/well) and counted after 72 hours of cultivation. In order to test whether varying serum concentrations influenced the population doubling time, cells were cultured in α-MEM supplemented with 2, 5 or 10 % FCS respectively. As indicated in Figure 12, RAW 264.7 cells were proliferating faster at higher serum concentrations. The averaged population doubling times were 34 h (± 3 h) at 2 %, 26 h (± 3 h) at 5 % and 22 h (± 4 h) at 10% FCS supplementation. In another experiment where the population doubling time was followed for two weeks at 10 % FCS addition (PD10 to PD27) the averaged PDT was higher (26 h; data not shown).

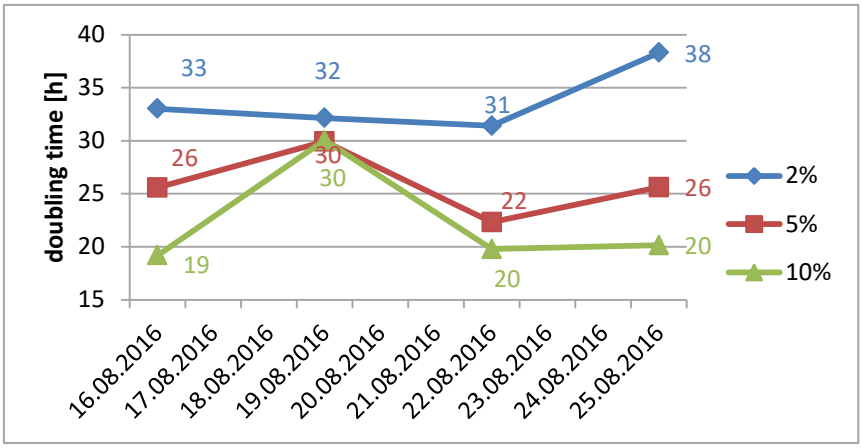

Figure 12: FCS concentration influences population doubling time.
A higher FCS concentration was linked to an increased population doubling time. The averaged PDT for the blue line (2 % FCS) is 34 h, for the red line (5 % FCS) 26 h and for the green line (10 % FCS- which was the usual serum concentration for all experiments) 22 h. At the start cells were at PD 9.

7.2 Osteoclast differentiation experiments

7.2.1 Cell density as an important parameter in osteoclast differentiation

In the field of bone research it is generally accepted that the cell density is a key parameter in osteoclast formation and this was also shown for RAW 264.7 differentiation experiments [50]. Due to this fact an optimal cell seeding number had to be determined and started with the comparison of 50,000 against 25,000 cells per 1.9 cm^2 (24-well plate). While the cultivation area was completely overgrown with the higher seeding number after one week, still some space was left with the 25,000 cells/well when treated with 20 ng/ml of RANKL (data not shown) (R&D; TR). The influence of cell density was further examined by using even lower cell seeding numbers (3,125 to 25,000 per 1.9 cm^2) and showed a clear correlation to the formation of TRAP (+) cells after 7 days of cultivation (Figure 13; A-H). As expected, cells of the control remained unstained while increased numbers of TRAP (+) cells were related to lower cell seeding numbers. This was also confirmed by testing the enzymatic activity of TRAP shown in the diagram below (Figure 13; I).

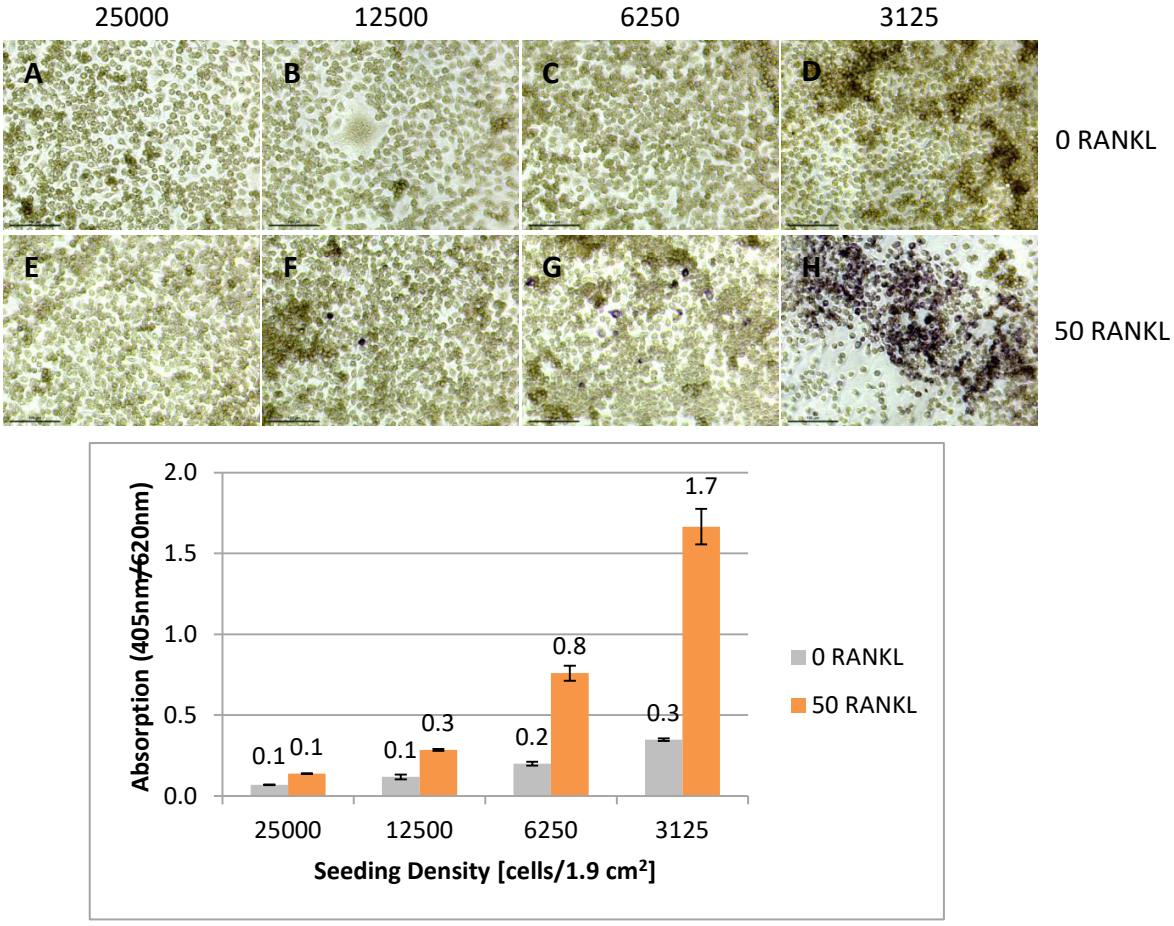

Figure 13: Cell density has a major impact on the generation of TRAP (+) cells.
Different numbers of RAW 264.7 cells were seeded into a 24-well plate and treated with RANKL (50 ng/ml) for 7 days. TRAP staining and assay were then performed to study the enzyme activity of the tartrate-resistant acid phosphatase. Higher TRAP activity was linked to lower cell seeding numbers. Control cells (medium only) remained TRAP (-). Data are normalised to 25,000 cells and shown as mean values ± SD (n_b= 1; n_t=3)

Since differentiation and proliferation factors such as TGF-β_1 had a major impact on cell proliferation this had to be considered in the determination of the optimal cell seeding number. It was advisable to follow the changes in the cell confluence over the whole experiment and retrospectively a final confluence of 70 -80 % yielded the best results in osteoclast formation.

7.2.2 Population Doublings (PD) and RAW 264.7 differentiation potential

During the first period of the study RAW 264.7 cells were grown for many passages. At PD 69 cells seemed to change morphology with the appearance of a more spread or enlarged phenotype.

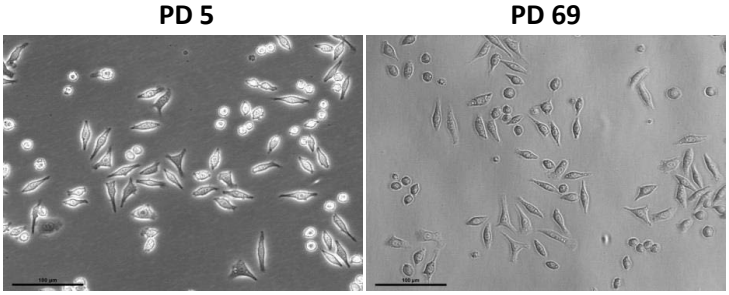

Figure 14: Morphological comparison of PD 4 against PD 69.
At PD 69 cells showed an enlarged phenotype compared to PD 5.

To test whether the Population Doublings affect the differentiation potential of RAW 264.7 cells PD 4 was compared against PD 23. Therefore cells were treated with RANKL (50 ng/ml) for 7 days and stained for TRAP. While PD 4 cells remained unstained upon RANKL treatment PD 23 cells responded to the stimulation by the development of TRAP (+) cells and small pre-osteoclasts. Unexpectedly, even some of the control cells of PD 23 turned purple. During the whole study this was the only time control cells showed TRAP activity.

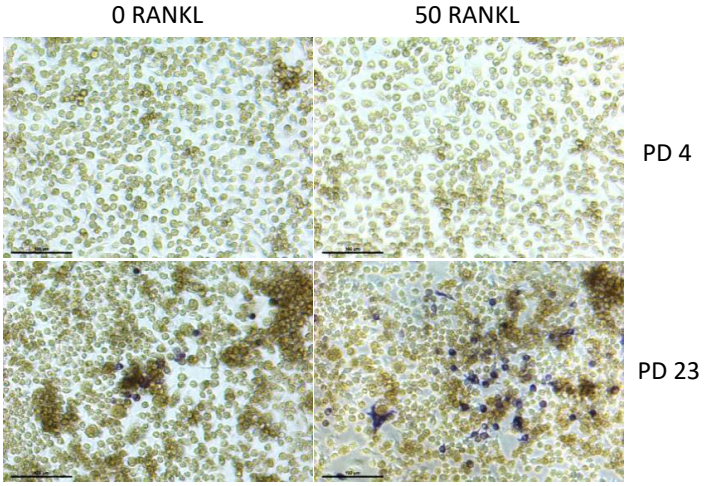

Figure 15: Differentiation potential of PD 4 against PD 23.
While RANKL-treated cells of PD 4 remained unstained PD 23 cells showed TRAP activity which can be seen by the purple colour. Unexpectedly, few control cells of PD 23 were also TRAP (+).

7.2.3 RANKL: key factor of osteoclastogenesis

The most essential differentiation factor for osteoclast formation is RANKL and several recombinant products can be ordered from different suppliers. During this study three products were used and tested regarding their osteoclast formation effectiveness. Since RANKL from R&D Systems (462-TR) performed better than a product of PeProTech (Figure 16; A-C) the former product was chosen for further experiments. However, it turned out that RANKL-462-TR works only properly in combination with a cross-linking antibody which was not used in this study. For that reason another product from this company, which was not dependent on the addition of such an antibody (R & D Systems; 462-TEC) was ordered and turned out to work better than RANKL-TR (see Figure 16; D).

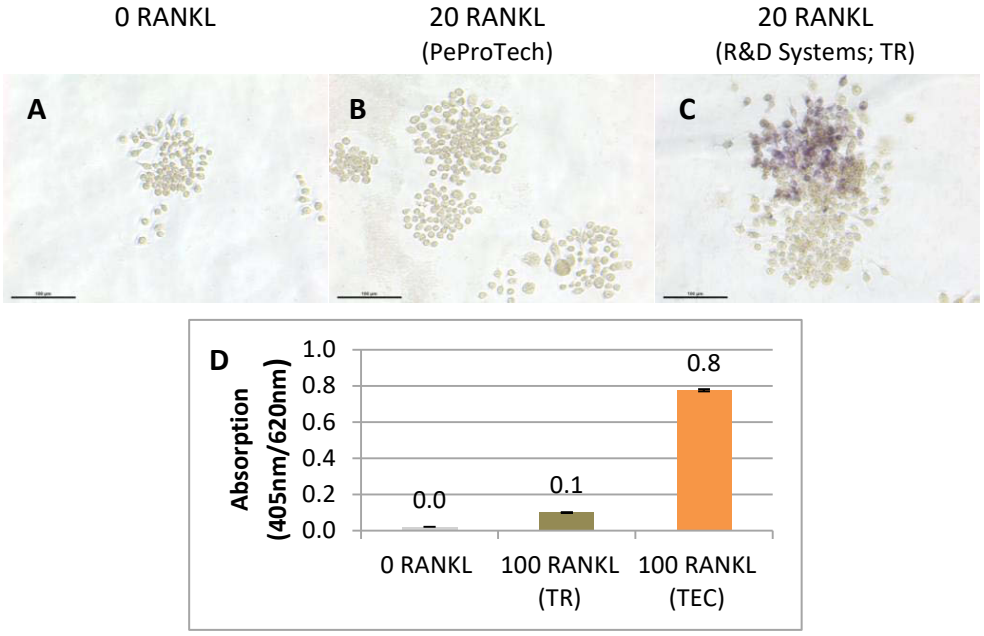

Figure 16: RANKL product comparison.

[A-C] Cells treated with 20 ng/ml RANKL from PeProTech **(B)** or R&D Systems; TR **(C)** for 7 days. TRAP (+) cells developed only with RANKL-TR **[D]** RANKL-TEC performed better than RANKL-TR since the latter product is dependent on a cross-linking antibody which was not used in this study. Data are shown as mean values ± SD (n_b= 1; n_t=3).

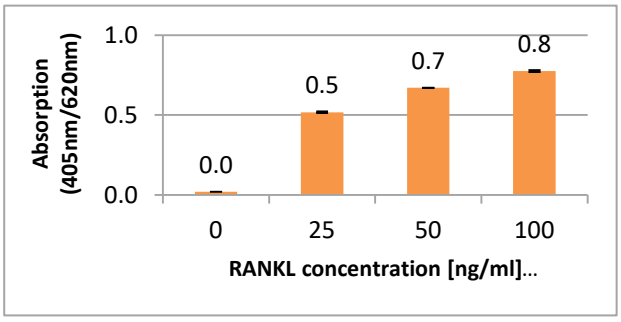

Figure 17: Relationship between RANKL-concentration and TRAP activity.

High RANKL-concentration was linked to a higher activity of TRAP but did not lead to the formation of any osteoclasts in DMEM high glucose. Data are shown as mean values ± SD (n_b= 1; n_t=3).

The next step was to examine if osteoclast formation was RANKL concentration-dependent and to determine the lowest final concentration where osteoclasts still developed. Treatment with 0, 25, 50 and 100 ng/ml of RANKL (R&D; TEC) showed a dose-dependent activity of TRAP (Figure 17) but did not lead to the formation of multinuclear cells in DMEM high glucose.

7.2.4 TGF-β_1 enhances osteoclast formation

To test whether TGF-β_1 enhances RANKL-induced osteoclast formation, RAW 264.7 cultures were treated with RANKL alone or in the presence of 3.3 ng/ml TGF-β_1. The concentration of TGF-β_1 was chosen due to literature research and preliminary experiments (data not shown). While cells treated with RANKL alone remained almost completely TRAP (-) the addition of TGF-β_1 increased the formation of TRAP (+) cells substantially. At a concentration of 100 ng/ml RANKL the addition of TGF-β_1 led to the formation of small pre-osteoclasts as can be seen in Figure 18 (E). An increase in the enzymatic activity of TRAP could be also confirmed by the photometric assay (Figure 18; F). Furthermore the addition of TGF-β_1 increased the expression levels of early and late osteoclast marker genes as can be seen in

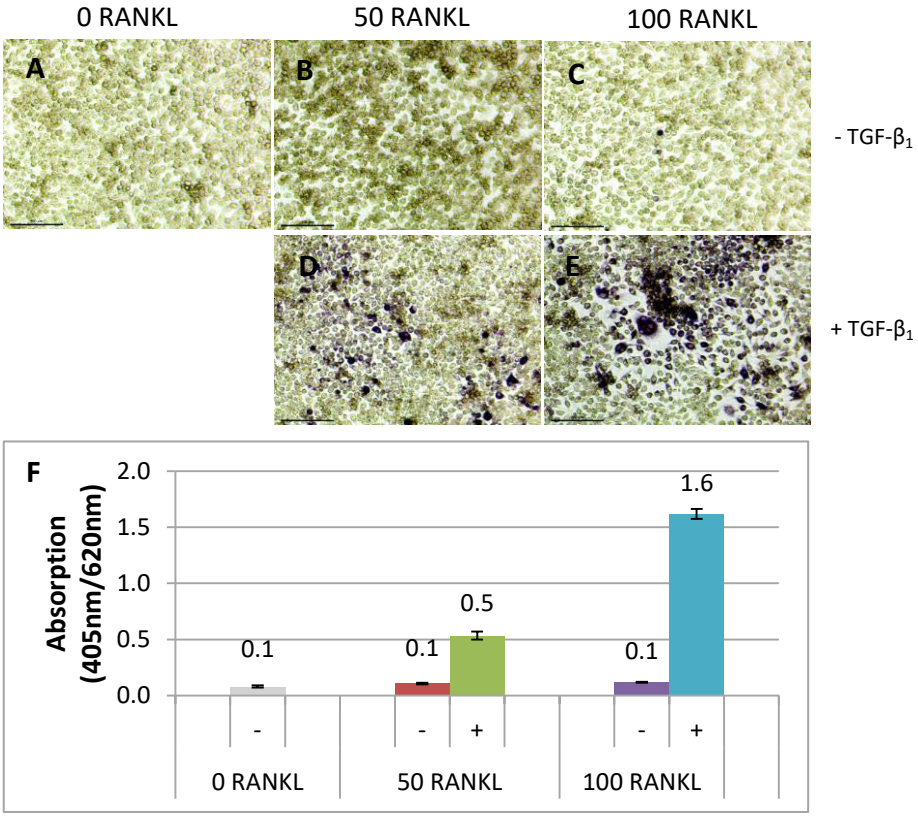

Figure 18: Effect of TGF-β1 on osteoclast formation.
[A-E] **The addition of TGF-β1 (indicated by + symbol) increased the formation of TRAP (+) cells substantially as well as the activity of TRAP [F].** Data are shown as mean values ± SD (n_b= 1; n_t=3).

Figure 19 (A-E). Cathepsin K and TRAP belong to early osteoclast marker genes [51] but are also expressed by dendritic cells [52]. Therefore more specific osteoclast marker genes were

needed. The expression of Atpv60d2 is bifunctional: On the one hand Atpv60d2 is an important fusion molecule, necessary for osteoclast development, and on the other hand it is part of the vacuolar H^+-ATPase needed for resorption pit acidification [53]. The expression of OSCAR is specific to osteoclasts [52]. Calcitonin receptors are only expressed in mature osteoclasts and considered as late marker genes [51]. The osteoclast enhancing effect of TGF-β_1 was observed in all subsequent experiments shown in Figures 20, 21 and 22 (comparison of 20 ng RANKL plus/minus TGF-β_1).

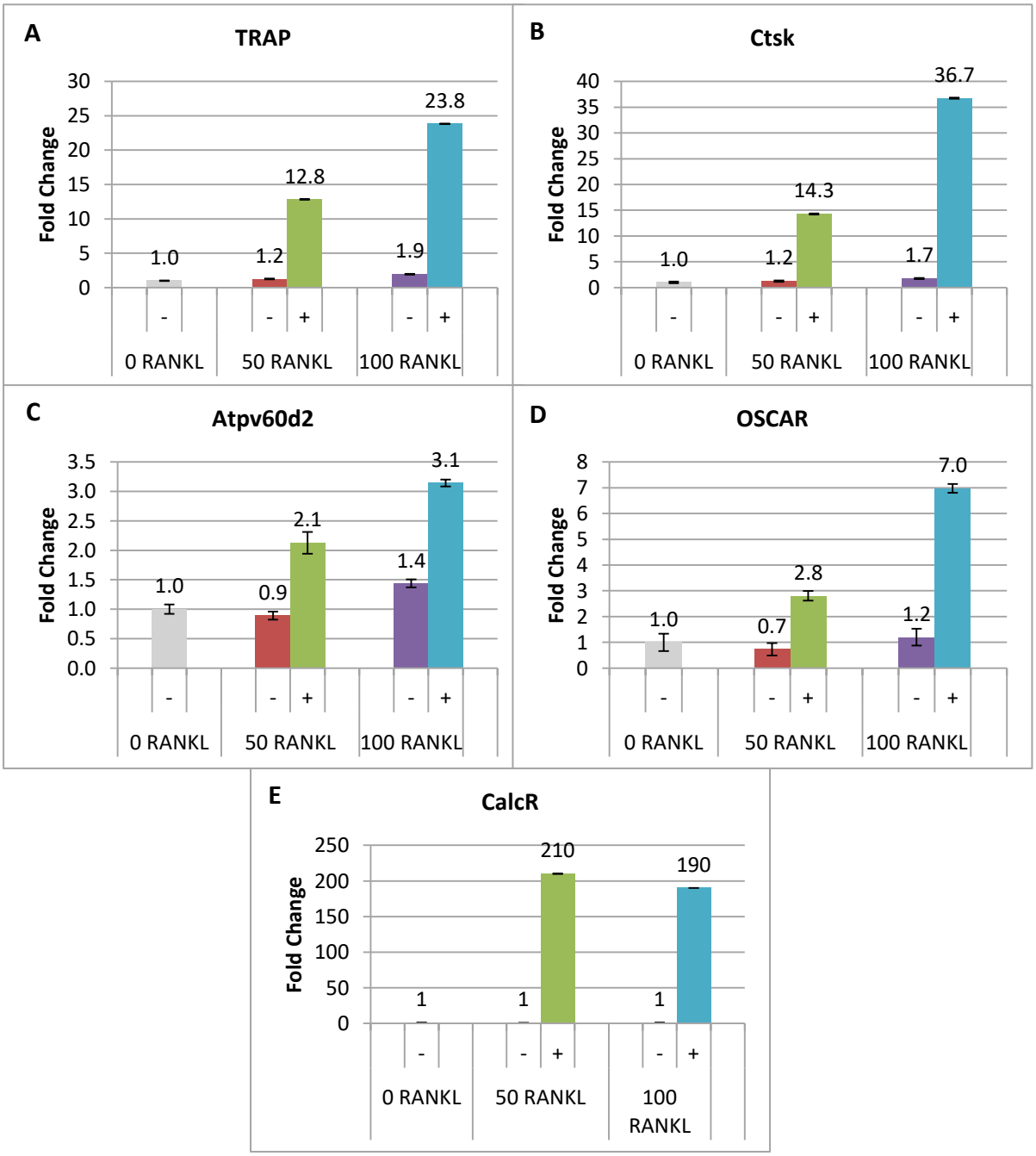

Figure 19: Addition of TGF-β1 leads to upregulation of osteoclast marker genes.

When RANKL-stimulation alone was compared with TGF-β1 treatment (indicated by a + symbol) early (A; B), middle (C) and late (D ;E) osteoclast markers were upregulated. The target mRNA was normalised to β-actin mRNA. Data are shown as mean values ± SD (n_b = 1; n_t = 3).

7.2.5 DMEM high-glucose suppresses osteoclast differentiation

Since osteoclast formation and bone resorption are two highly energy-consuming processes [16] for a long time it was not questioned if DMEM high glucose was the right medium of choice. With its high glucose and L-glutamine content it seemed to be perfectly suitable for osteoclast differentiation. However, the publication of Xu et al states that high glucose inhibits RANKL-induced osteoclast differentiation by impairing cell-cell fusion of precursor cells [54]. For that reason differentiation capacity of RAW 264.7 cells was compared by cultivation in DMEM high glucose or α-MEM respectively.

TRAP staining was performed 5 days after the start of differentiation to estimate the number of osteoclasts which have already been seen through microscopic examination. As shown in Figure 20, treatment with RANKL and TGF- β_1 induced the formation of large osteoclast when cells were cultivated in α-MEM. In contrast the same treatment settings in DMEM led to the formation of mononuclear TRAP (+) cells only. Interestingly, a high number of osteoclasts was dependent on the addition of TGF- β_1, supporting some earlier results described in 7.2.4.

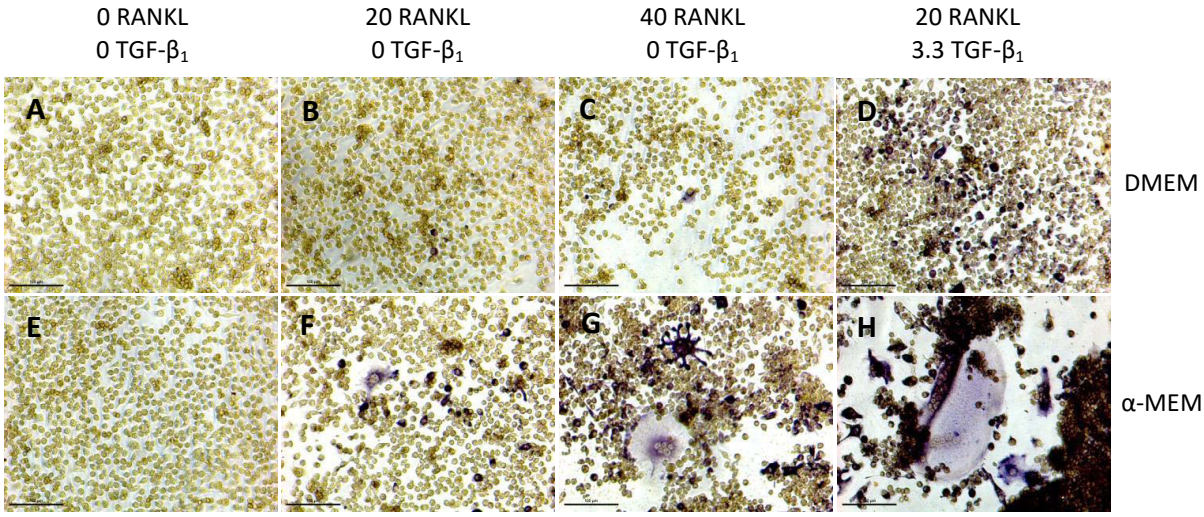

Figure 20: TRAP staining of DMEM high glucose against α-MEM differentiation on day 5.
Large osteoclasts developed only in α-MEM cultivation with the addition of TGF-β_1. RANKL-induction alone had very little impact on osteoclast generation in DMEM while dose-dependently some mononuclear TRAP (+) but few osteoclasts were formed in α-MEM.

In line with these optical impressions were the absorption measurements which demonstrated a higher TRAP activity in α-MEM cultivation for all treatment conditions (excluding the controls). High absorption values in DMEM (20 ng/ml RANKL; 3.3 ng/ml TGF-β_1) were due to the formation of many mononuclear TRAP (+) osteoclast precursor cells.

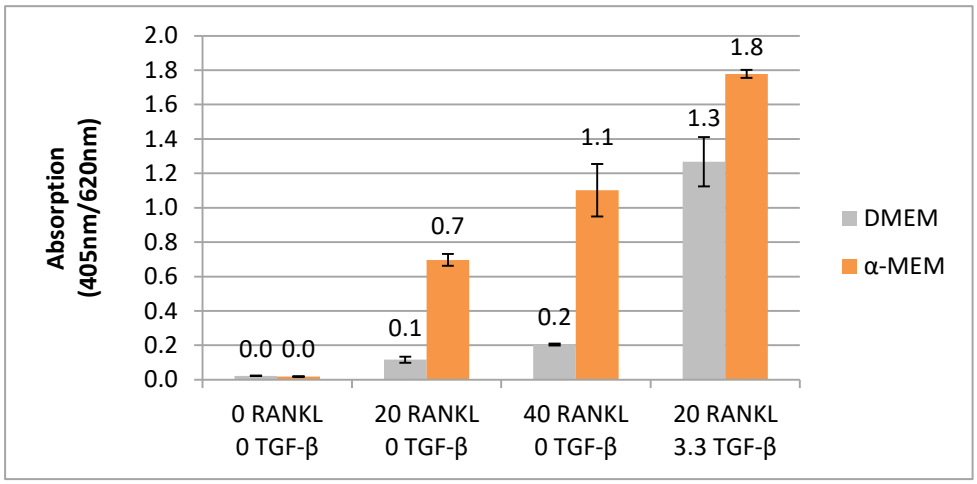

Figure 21: TRAP activity in DMEM high glucose vs. α-MEM cultivation.
The addition of differentiation factors increased the TRAP activity mainly in α-MEM cultured cells. Although the addition of TGF-β_1 had a positive effect on enzyme activity in both culture media the highest absorption value was reached in α-MEM. Data are shown as mean values ± SD (n_b = 1; n_t = 3).

To examine if osteoclast differentiation was inhibited due to an impaired fusion process the gene expression level of Atpv60d2 was analysed. In accordance with the results of Xu et al, the Atpv60d2 expression level was lower when cells were cultured in high glucose medium (DMEM) compared to low glucose cultivation (α-MEM) at all treatment conditions, although the basal expression of Atpv60d2 in the control (0 ng/ml RANKL, 0 ng/ml TGF- β1) was higher in DMEM (see Figure 22; A). All evaluated osteoclast markers were strongly upregulated in α-MEM compared to high glucose treatment which highlights the importance of low glucose concentration for the formation of multinucleated osteoclasts.

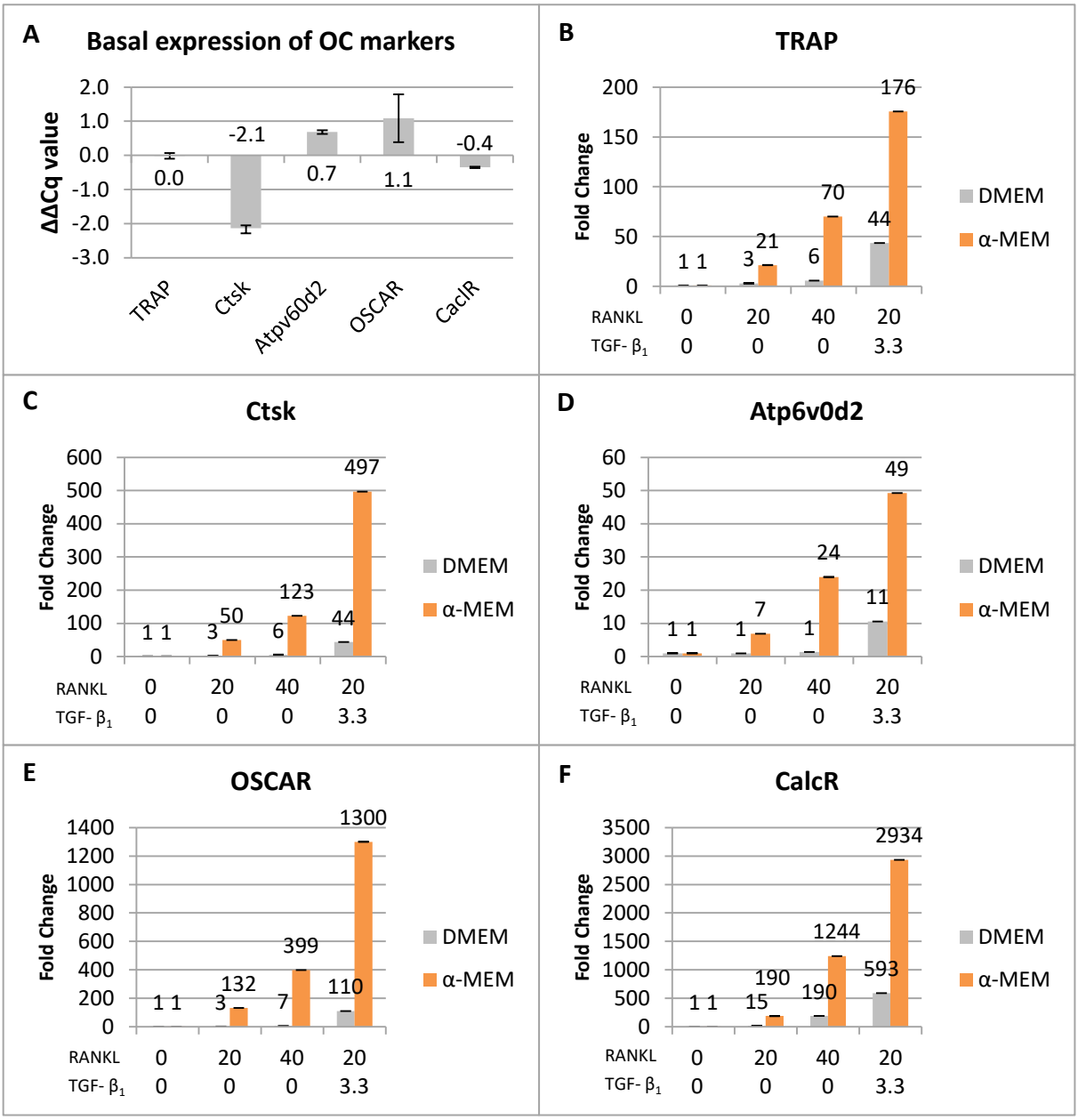

Figure 22: Osteoclast marker genes stay low in DMEM high glucose.

(A) Basal expression levels of osteoclast marker genes in the control (0 ng/ml RANKL, 0 ng/ml TGF-β_1) normalised to α-MEM cultivation. **(B-F)** While there was a high upregulation of all marker genes when cells were cultured in α-MEM this was not the case for DMEM high glucose cultivation. In comparison to α-MEM, DMEM high glucose seemed to suppress early osteoclast markers **(B, C)** but most importantly, the fusion molecule Atpv60d2 **(D)** which was a possible explanation why osteoclasts did not maturate. The target mRNA was normalised to β-actin mRNA. Data are shown as mean values ± SD

7.3 Transfection experiments

7.3.1 Transfection optimisation

Optimal miRNA transfection into RAW 264.7 cells combines high transfection efficiency with low cytotoxicity. Parameters, such as the cell viability, transfection agent and RNA concentration are known to critically affect the outcome of the experiment and can vary between different cell types.

In order to transfect RAW 264.7 cells with miRNA precursors two different methods (electroporation and a lipid-based agent) were tested and compared regarding transfection efficiency 48 h after transfection. According the NEON instruction manual 225 pmol of fluorescence-labeled pre-miR (FAM or Cy3) were used for the transfection of 600,000 cells using a 10 µl tip. We observed low viability in RAW 264.7 cells after electroporatic transfection with this RNA concentration. In contrast, using lipid-based transfection (siPORT™ NeoFX™ Transfection Agent, 30 nM) cells retained high viability, which is why it was selected as the method of choice. For the sake of completeness it should be noted that also lower concentrations of miRNA precursors were transfected via electroporation at which the cells remained viable but did not show any fluorescence signal meaning cells did not take up the RNA cargo (data not show). In the next step, transfection efficiency was analysed. Unexpectedly, the detection of FAM-transfected cells showed inconsistent results. During imaging with a fluorescence microscope cells appeared fluorescent. This was also confirmed by the transfection assay using the Luna-FL™ Dual Fluorescence Cell Counter indicating a high transfection efficiency of 84.5 %. However, it was not possible to detect the FAM signal via flow cytometry whereby a technical problem or wrong laser/filter/detector selection can be excluded since FAM detection worked with another cell type using the same settings (data not shown). Therefore it was necessary to use another indicator which allowed the measurement of transfection efficiency with flow cytometry, namely Cy3. Figure 23 shows a peak shift of Cy3-transfected cells with higher FL-2 intensities compared to the negative control. The transfection efficiency was determined to a value of about 47 %.

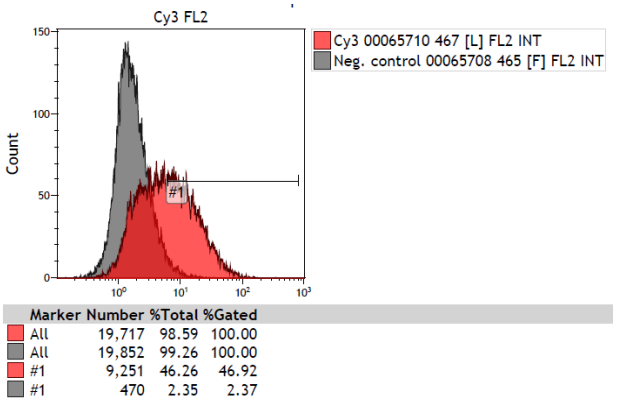

Figure 23: Determination of transfection efficiency.
As expected Cy3-transfected cells showed higher fluorescence intensities as the negative control-transfected cells resulting in a peak shift. Transfection efficiency was about 47 %.

7.3.2 Overexpression analysis of miRNAs

Although the intracellular uptake of miRNA precursors was already confirmed through fluorescence detection, additionally the successful conversion of pre-miRNAs into mature miRNA had to be checked using the quantitative real-time PCR method.

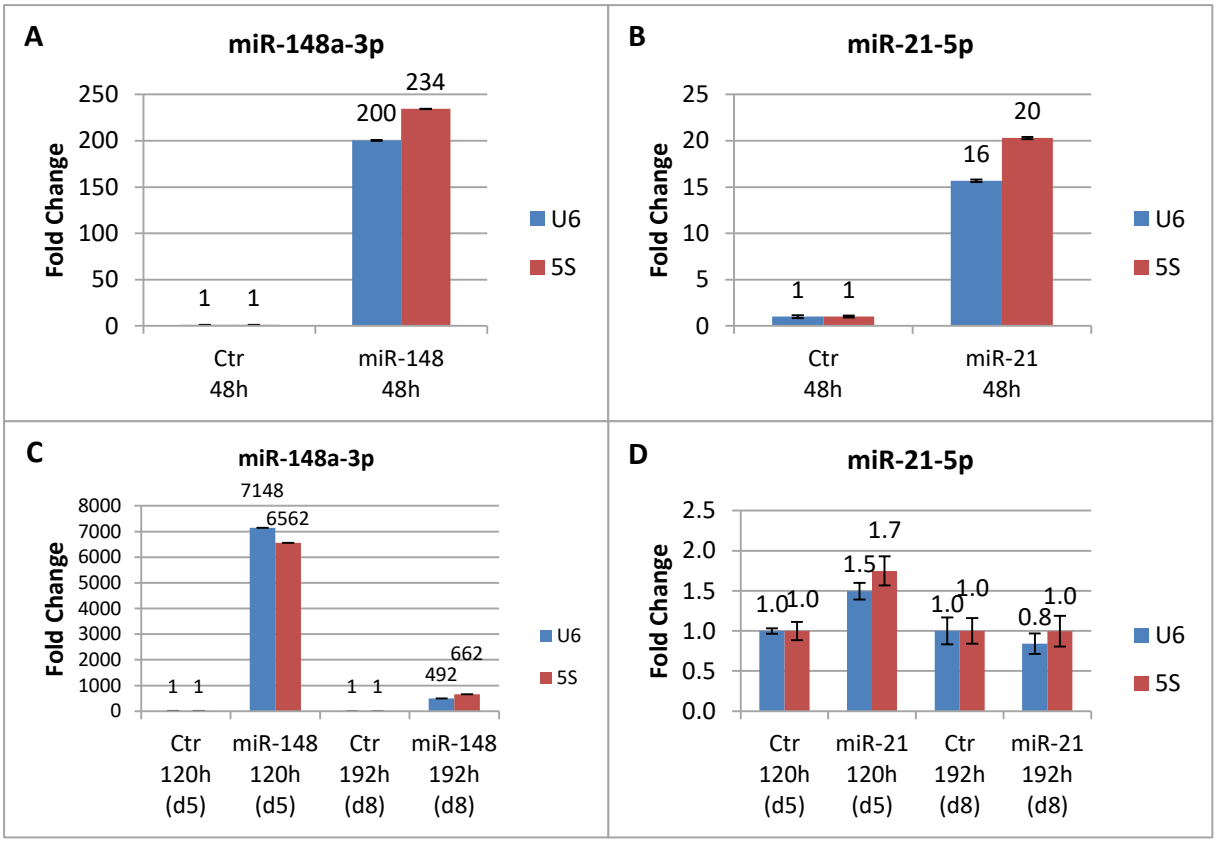

Figure 24: Overexpression analysis of miR-148a-3p and miR-21-5p at different time points.
(A) 48 h after transfection the expression level of miR-148a-3p was high with fold changes of 200 (U6) and 234 (5S) respectively. **(B)** Overexpression of miR-21-5p was lower compared to miR-148a-3p with values of 16 (U6) and 20 (5S) but still noticeable. This large difference of fold change values can be explained due to the higher basal expression of miR-21-5p with a Cq-value of about 24 in contrast to miR-148a-3p were the Cq-value was not detectable in control cells. In contrast basal miR-148a-3p expression was very low and could not be detected. Overexpression levels were analysed in another experiment on day 5 and 8, where the cells were treated with differentiation medium from day 2 on (C, D). **(C)** Overexpression of miR-148a-3p on day 5 was very high but decreased strongly until day 8, still showing high overexpression values. **(D)** On day 5 overexpression of miR-21-5p was very little and on day 8 there was no difference between control and transfected-cells anymore. The target miRNA was normalised to U6 and 5S. Data are shown as mean values ± SD (n_b = 1; n_t = 3).

Figure 24 shows the overexpression levels of miR-148a-3p and miR-21-5p. While miR-148a-3p showed high overexpression with fold changes of > 200-fold after 48 h of transfection, the miR-21-5p overexpression was lower but still noticeable. The large difference in these values can be explained by the fact that miR-148a-3p basal expression is much lower (Cq undetectable) than miR-21-5p basal levels (Cq ~ 24). Furthermore the expression levels of these miRNAs were analysed in another experiment on day 5 (120 h) and 8 (192 h) after transfection. Importantly these cells were treated with differentiation medium (20 ng/ml RANKL-TEC, 3.3 ng/ml TGF-β_1) from day 2 on. The overexpression level of miR-21 was

quite low on day 5 and decreased further so that no difference could be seen between the control and transfected cells on day 8 anymore. Interestingly, overexpression of miR-148a-3p was very high on day 5 but decreased rapidly until day 8, still showing high fold change values. In general the normalised fold change values to 5S and U6 matched very well indicating constant expression of these two reference genes in this model.

7.4 Validation of the osteoclast *In Vitro* model

After the optimisation of RAW 264.7 differentiation and transfection procedures the model was tested by the introduction of miR-21-5p and miR-148a-3p which are both described as osteoclast differentiation enhancers [32, 40]. As shown in Figure 25, large osteoclasts developed after 6 days of differentiation (α-MEM; 20 ng/ml RANKL + 3.3 ng/ml TGF-β_1) in the control and miR-21-transfected cells. Osteoclasts were smaller and less developed in the miR-148-transfected cells. Notably, many cells died after the differentiation start, especially in the miR-148 group, which might strongly have influenced the experiment outcome.

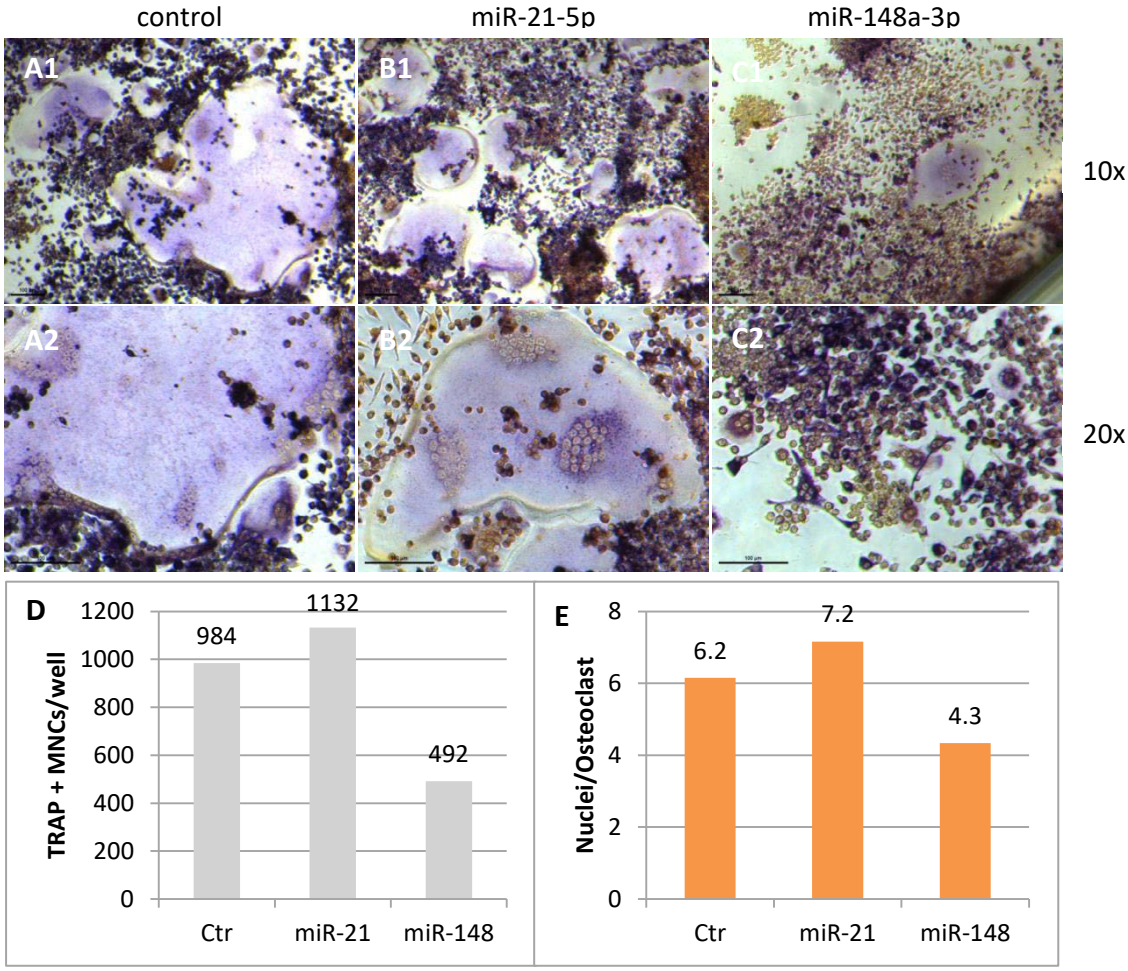

Figure 25: Effects of miR-21-5p and miR-148a-3p on osteoclast differentiation.
RAW264.7 cells were transfected with negative control **(A)**, miR-21-5p **(B)** or miR-148a-3p **(C)** using siPORT NeoFX transfection agent and treated with RANKL (20 ng/ml) and TGF-β_1 (3.3 ng/ml) in α-MEM for 6 days. (D) Number of TRAP (+) multinuclear cells per well (24-well plate). (E) Average nuclei number of osteoclasts. Pictures A1, B1 and C1 are 10x and A2, B2 and C2 are 20x magnified.

Another problem in the case of miR-148a-3p was an uneven cell distribution (Figure 25, C1), where the cell density was much higher at the edges. A1 shows the largest osteoclast that has formed with a size up to 600 µm and an extraordinary high number of nuclei (more than 100). Interestingly, after cell-cell fusion the nuclei were positioned in the middle first (Figure 25, B2) and were moving to the edge when the osteoclasts maturated (Figure 25, A2).

TRAP activity was found to be saturated (beyond the upper detection limit) for all three conditions. Therefore, no distinction could be made between the groups (data not shown) and biomarker expression was analysed by qPCR. MiR-21-5p and miR-148a-3p led to an increase in all osteoclast marker genes on day 3 after differentiation induction. In contrast, on day 6 biomarker expression was highest in control transfected cells.

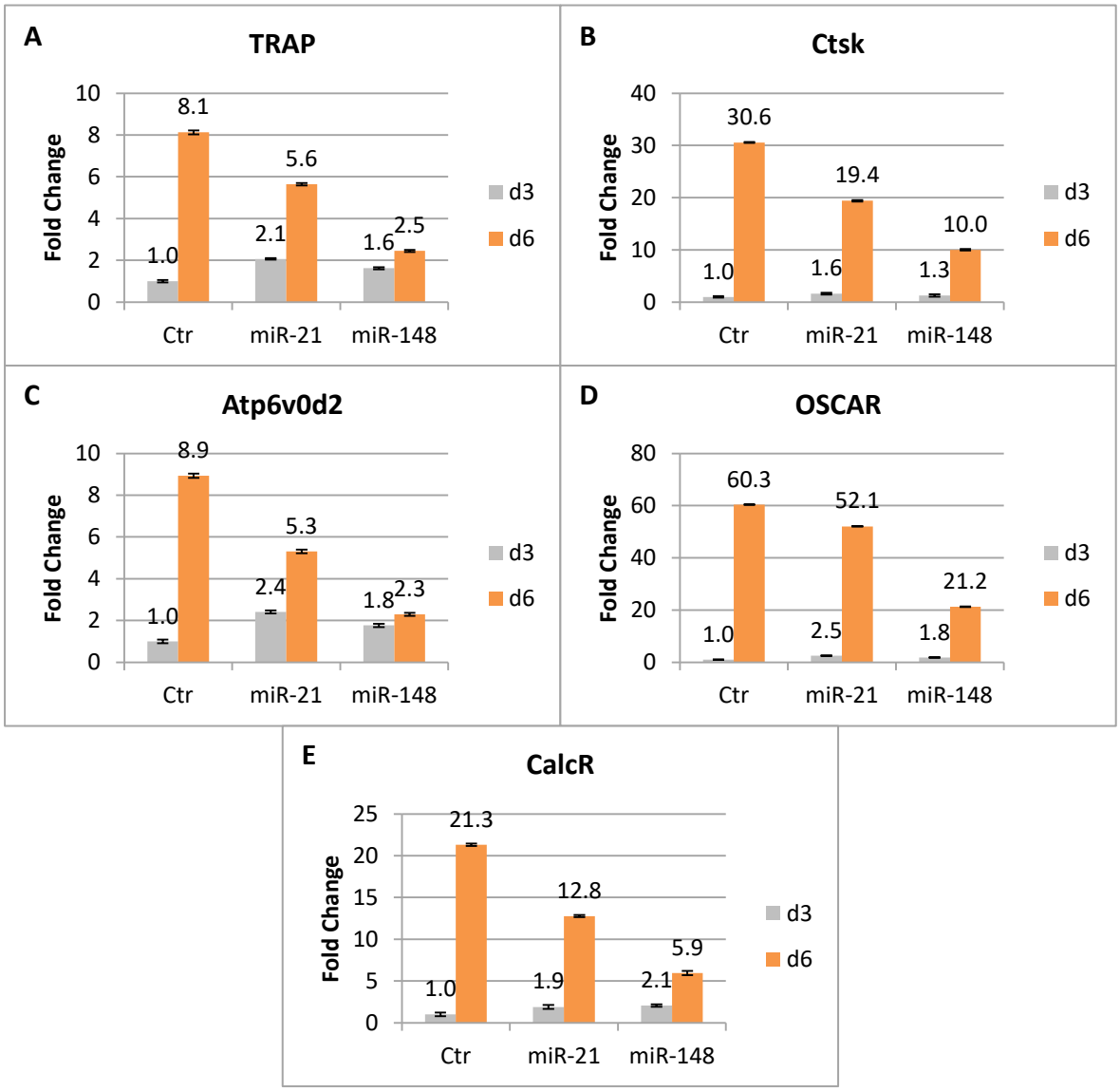

Figure 26: Osteoclast marker gene expression after miR-21-5p and miR-148a-3p transfection

Although all osteoclast marker genes were upregulated on day 6 in comparison to day 3, highest levels were reached for the negative control at that time. This was not expected since miR-21-5p and miR-148a-3p are known osteoclast enhancers. Only on day 3 miR-21 and miR-148 seemed to have a positive effect on osteoclast marker expression. The target mRNA was normalised to β-actin mRNA. Data are shown as mean values ± SD (n_b = 1; n_t = 3).

8 Discussion

Until today, the importance of miRNAs in the regulation of bone homeostasis but also bone diseases such as osteoporosis was confirmed by several studies [23, 27, 32]. To gain insights into the functions and effects of miRNAs on osteoclastogenesis, the establishment of an *In Vitro* model was necessary. Nowadays, osteoclast differentiation can be easily induced by the addition of recombinant RANKL (and M-CSF) to osteoclast precursor cells. However, there are two main possibilities regarding the cell source: One option are so called „primary cells" from bone marrow or blood, but these cells must be isolated first, are limited in terms of availability and assay performance is influenced by donor-variation. Therefore many research groups use an immortal, monocyte cell line called RAW 264.7 which was also decided to use in this study.

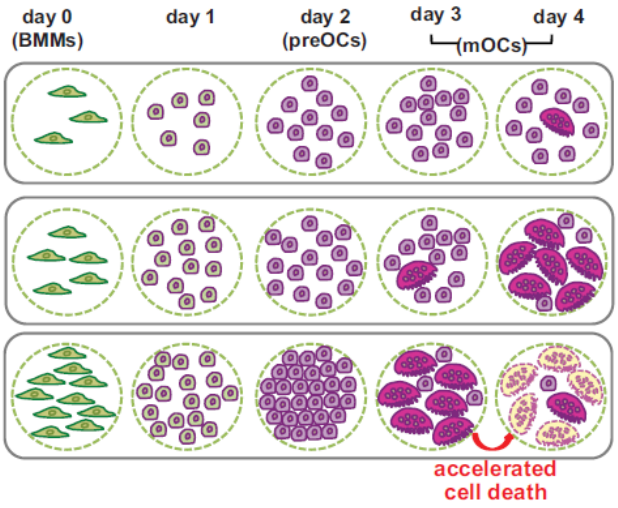

Figure 27: Cell density is an important parameter in osteoclast differentiation.
While too low cell densities results in the formation of few osteoclasts, too high cell densities lead to earlier osteoclast generation but accelerated cell death. [© Ikeda et al 2015]

At the beginning of this work, intensive literature research was performed to identify several critical parameters for osteoclast formation from RAW 264.7 cells. In this study, we tested the impact of these parameters and gradually optimized the differentiation protocol. As described by Rahman et al one key parameter in osteoclastogenesis is the cell density [50]. For that reason several cell seeding densities (3,125, 6,250, 12,500, 25,000, 50,000 per 1.9 cm^2) were compared regarding their osteoclast forming efficiency showing that a final cell confluence of 70 to 80 % yielded the best results. The determination of the cell seeding number seemed to be trivial at first. However, the addition of TGF-β_1 (reduced cell proliferation) and the cultivation period (thus the timing of analysis) were two strongly influencing factors. An optimal density was achieved with the seeding of 25,000 /1.9 cm^2 (24-well plate) when 20 ng/ml RANKL-TEC and 3.3 ng/ml TGF-β_1 were added to α-MEM. It is

widely believed that RANKL has anti-proliferative properties and that terminal cell differentiation is linked to cell cycle exit [50]. However, Rahman et al. reported that RANKL enhances proliferation during the first 48 h after differentiation start following an anti-proliferative effect. Here, we observed that RAW cells are proliferating during the first days after RANKL addition and that only TGF-β_1 treatment inhibits proliferation. This observation is in agreement with Rahmans´ concept stating that only a sufficient number of precursor cells enables cell-cell contact and the process of cell fusion. Interestingly, this research group also described an upper limit of cell density, which on one hand induces earlier osteoclast formation but on the other hand leads to accelerated cell death (see Figure 27). We observed a similar effect in this study since osteoclasts did not develop when the cells were reaching over 80 % of confluence. Thus, the fundamental impact of cell density on the outcome of osteoclast formation has to be considered when interpreting results. Any drug or miRNA affecting cell proliferation will have a major impact on the number of pre- and mature osteoclasts. This might also have critically influenced the outcome of the validation experiment.

Although RAW 264.7 cells have a common origin (suggesting a homogenous population), some publications reported heterogeneity among these cells [51, 55] and an age-dependent effect on the osteoclast forming potential, because early and late passages tend to reduce osteoclast numbers [46]. Therefore, we tested cells of PD 4 against PD 23 and found out that only cells of the higher PD were generating TRAP (+) cells. One possible explanation could be that cells at low PD are more prone to proliferation instead of differentiation in order to provide enough precursor cells as already described before. With regard to high PD levels the genetic instability of immortal cell lines [56], connected to phenotypical changes might be another reason for a lack of responsiveness to differentiation factors.

From beginning on it was obvious that RANKL was needed as it is described as the key factor of osteoclast differentiation. However, several recombinant products had to be compared regarding their efficacy in this model. Although RANKL-TEC performed best it did not lead to the formation of multinuclear cells in DMEM high glucose but instead only TRAP (+) mononuclear cells, suggesting a failure in the important process of osteoclast precursor fusion. A striking aspect was also that cells seemed to continue proliferation until the endpoint of analysis about 7 days after RANKL addition. We found that this strong proliferative nature could only be attenuated by the addition of TGF-β_1.

Actually, TGF- β_1 is one of the most prominent regulatory cytokines of the immune system that controls inflammatory responses by the activation of lymphocytes, natural killer cells, dendritic cells, macrophages and other immune cells [57]. Since osteoclasts are (like immune cells) of hematopoietic origin, these cells are the most obvious link between the

immune and bone system (field of osteoimmunology) [57]. Based on this knowledge it is not surprisingly that TGF- β_1 is also an important regulator in bone cell communication. However, the role of TGF-β_1 as costimulatory cytokine in osteoclastogenesis is complex and controversial [58]. When hematopoietic precursor cells were stimulated with RANKL and M-CSF, the addition of TGF-β_1 enhanced osteoclast formation [59, 60]. Fuller et al claimed TGF-β_1 as an indispensable factor for osteoclast formation and survival since its neutralisation by a recombinant soluble TGF-β receptor II abolished the development of bone-resorbing cells completely [61]. TGF-β_1 was reported to directly induce NFATc1, the key transcription factor to activate osteoclast marker genes [62] and to upregulate RANK [63] thereby facilitating RANKL-binding. Otherwise, when osteoblasts were cocultured with osteoclast precursors TGF-β_1 inhibited osteoclastogenesis [64]. In another coculture system a dose-dependent effect of TGF- β_1 was recognized [65]. While a low concentration (~10^{-4} ng/ml) stimulated osteoclast differentiation a high concentration (2 ng/ml) was inhibiting due to the downregulation of M-CSF and the upregulation of osteoprotegerin [65]. In the present study however only the supplementation of RANKL with TGF-β1 (in α-MEM) led to the formation of mature osteoclasts suggesting an essential role of this cytokine in osteoclast formation (see Figure 18, Figure 20 (F,H) and Figure 21 (20 ng/ml RANKL ± TGF- β_1)).

Here, we found that the key to successful osteoclast differentiation was a switch from DMEM high glucose to α-MEM with low glucose concentration (see

Table 2). The selection of the culture medium was not questioned for a long time since it was recommended as the basal medium for RAW 264.7 cells and seemed to be perfectly suitable for osteoclast differentiation, which was described as a highly energy demanding process by Ikeda et al. They reported an upregulation of the glucose transporter (Glut 1) and glycolytic genes such as hexokinase, phosphofructokinase and pyruvate kinase during osteoclast differentiation [16]. In addition Slc1a5, the transporter of L-glutamine, and Glutaminidase, which functions in the conversion of glutamine to glutamate, were both upregulated during osteoclast development [16]. All these findings reminded us to choose DMEM high glucose as long as reading the publication of Xu et al which stated that high glucose was inhibiting RANKL-induced osteoclastogenesis by the impairment of precursor cell fusion [54]. For that reason the performance in DMEM high glucose and α-MEM was compared. In general, TRAP activity and the expression of further evaluated osteoclast marker genes was clearly higher in α-MEM cultured cells. This was not due to cell density differences but rather due to another reason. Especially the formation of multinucleated cells seemed to be inhibited by DMEM high glucose suggesting a failure of cell-cell fusion. This was supported by low Atpv60d2 expression compared to low glucose cultures (α-MEM), which was also described

by Xu et al. The present study however cannot exclude an inhibiting effect of the high L-glutamine content.

When thinking about high glucose levels the first thing that comes into mind is another metabolic disease, namely diabetes, and interestingly diabetes patients have an increased risk of bone fracture [45]. Considering the results of this study and the findings of Xu et al the connection between diabetes and bone fractures seems to be logically. A decreased number of osteoclasts results in less removal of old or damaged bone [54]. On the other hand bone remodeling was already described as a highly regulated and coupled process between osteoblasts and osteoclasts, which means that less bone resorption is linked to a reduced production of new bone matrix and increases the risk of bone fractures. Additionally, it was recently shown that serum miRNAs can indicate the fracture risk of type 2 diabetes postmenopausal women [45]. Figure 28 shows the critical balance of bone formation and bone resorption. A disturbed balance decreases bone strength and causes bone diseases.

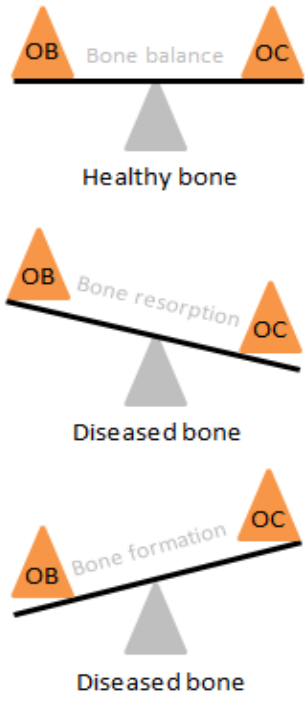

Figure 28: Bone balance.
In physiological state osteoblast and osteoclast activity are balanced. A disturbed balance favouring bone resorption or formation leads to reduced bone strength.

As a last step in the establishment of the osteoclast *In Vitro* model the effect of two osteoclastogenesis-promoting miRNAs, miR-21-5p and miR-148a-3p, were analysed. The interpretation of these results was, however, difficult since many cells died after the start of differentiation (especially miR-148a-3p cells) and led to an uneven distribution and different cell densities inside the culture well. One possible explanation for this observation is that miR-148a-3p overexpression resulted in cell apoptosis. This suspicion is supported by the fact that in the field of cancer research miR148a-3p was reported to promote apoptosis in colorectal cancer cells through targeting the anti-apoptotic gene Bcl-2 [66]. Three days after differentiation start, miR-21 and miR-148-tranfected cells showed higher expression of osteoclast marker genes than the control. Due to the fact that the control had the highest mRNA expression levels at the end and the osteoclast count resulted in little higher numbers of osteoclasts in miR-21 transfected cells, it is necessary to perform further validation experiments.

9 Conclusion and Outlook

During this master thesis an osteoclast *In Vitro* model was established from murine RAW 264.7 cells, in order to gain mechanistic insights into the function of miRNAs during osteoclastogenesis. In literature, several critical parameters of osteoclast formation have been published. However the methods varied between different research groups and laboratories. Therefore the big challenge was to optimise all parameters step by step, finding the right dosage for our system. In the end, large, multinucleated osteoclasts could be successfully generated. Nevertheless the model has to be further validated, in order to proof the effects of new miRNA candidates reliably.

10 Acknowledgements

After all those years of learning and studying now is the time to say thank you to many people:

First of all, I would like to express my deep gratitude to my supervisors Prof. Dr. Johannes Grillari and Dr. Matthias Hackl for giving me the chance to write my master thesis on such an interesting topic for TAmiRNA. Thank you both for your positive and motivated attitude, fruitful discussions and the continuous guidance. Matthias, thank you for taking the time to teach me whatever I wanted to know and for trusting in me and my skills.

I would like to thank Dr. Sylvia Weilner for introducing me into daily cell culture work and my colleagues Elisabeth Geiger, Susanna Skalicky and Moritz Weigl for their assistance and the very good working atmosphere.

Thanks to the Grillari-Aging group members (Luci, Hanna, Markus, Ingo, Regina, Lisa, Andre, Vera, David, Dominik, Clemens, Madhu, Fabian, Merima, Tonja and Barbara) for their support, constructive criticism and promising ideas. Especially, our weekly lab meetings and journal clubs were very helpful and contributed to success.

Furthermore I want to thank Dr. Matthias Wieser and the girls from Evercyte (Susanne, Teresa, Agata and Steffi) for their help.

Special thanks go to Dr. Martina Rauner from the Bone Lab Dresden. She was very kind in answering all my questions regarding RAW cells and their differentiation into osteoclasts. At this point I also want to thank our Italian friend Riccardo Paone who supported me in the lab with my osteoclast experiments during his stay in Vienna.

Finally, I want to thank my wonderful family and my friends for the continuous support and team spirit; and especially my parents for always standing by my side and making my dreams come true.

11 Abbreviations

° C	Degree Celsius
µl	Microliter
µM	Mikromolar
Ago	Argonaute
ATCC	American Type Culture Collection
Atp6v0d2	ATPase H+ Transporting V0 Subunit D2
BALB	Bagg albino
Bcl-2	B cell lymphoma gene 2
BMD	Bone mineral density
bp	Base pairs
CalcR	Calcitonin receptor
cDNA	Complementary deoxyribonucleic acid
CF	Carrier free
cm^2	Square centimeter
Cq	Quantitation cycle
Ctr	Control
Ctsk	Cathepsin K
DGCR8	DiGeorge syndrome critical region gene 8
dH_2O	Distilled water
DMEM	Dulbecco´s Modified Eagle Medium
DMSO	Dimethyl sulfoxide
DNA	Deoxyribonucleic acid
DXA	Dual-energy X-ray absorptiometry
ERK	Extracellular signal-regulated kinase
EV	Extracellular vesicle
FASL	Fas ligand
FC	Fold change

FCS	Fetal calf serum
FRAX	Fracture risk assessment tool
Fw	Forward
h	hours
Hsa	Homo sapiens
HSC	Hematopoietic stem cell origin
JNK	C-JUN N-terminal kinase
M-CSF	Macrophage-colony stimulating factor
min	Minutes
miRNA	Micro ribonucleic acid
ml	Milliliter
mM	Millimolar
Mmu	Mus musculus
mRNA	Messenger ribonucleic acid
MSC	Mesenchymal stem cell
n_b	Number of biological replicates
NFATc1	Nuclear factor of activated T-Cells 1
NFW	Nuclease free water
NF-κB	Nuclear Factor κ B Ligand
ng	nanogramm
Ng	Nanogramm
Nm	Nanometer
N_t	Number of technical replicates
NTC	No template control
OB	Osteoblast
OC	Osteoclast
OPG	Osteoprotegerin
OSCAR	Osteoclast Associated, Immunoglobulin-Like Receptor

PACT	Protein activator of PKR
PBMCs	Peripheral blood mononucleated cells
PBS	Phosphate Buffer Saline
PD	Population doublings
PDL	Population Doubling Level
qPCR	Quantitative real-time polymerase chain reaction
RANK	Receptor Activator of Nuclear Factor κ B
RANKL	Receptor Activator of Nuclear Factor κ B Ligand
Rev	Reverse
RISC	RNA-induced silencing complex
RNase	Ribonuclease
rRNA	Ribosomal RNA
RT	Room temperature
s	Seconds
SD	Standard deviation
snRNA	Small nuclear ribonucleic acid
TGF-β1	Transforming growth factor beta 1
TRAF6	TNF receptor associated factor 6
TRAP	Tartrate-resistant acid phosphatase
TRBP	TAR-RNA binding proteins
UTR	Untranslated region
V	Volt
WHO	World Health Organisation
α-MEM	Alpha- Minimum Essential Medium

12 List of figures

13 List of tables

14 References

(1) Lin JT, Lane JM. **Osteoporosis: a review**. Clin Orthop Relat Res. 2004:126–34.

(2) Lorentzon, M. and S. R. Cummings. 2015. "**Osteoporosis : The Evolution of a Diagnosis**."

(3) Pietschmann et al. 2012, **Principles of Osteoimmunology**: Molecular Mechanisms and Clinical Applications, Springer-Verlag, Wien

(4) Bilezikian JP, Raisz LG, Rodan RA, eds. **Principles of bone biology**. Second edition Volume 1, New York, 1996

(5) Marcus, R. et al., 2010. **Fundamentals of Osteoporosis**, Elsevier Inc.

(6) Boskey, A.L. & Coleman, R., 2010. **Aging and Bone**. , 89(12), pp.1333–1348.

(7) Guo, Dayong and Lynda F. Bonewald. 2009. "**Advancing Our Understanding of Osteocyte Cell Biology**." 87–96.

(8) Bonewald LF (2007) **Osteocytes as dynamic multifunctional cells**. Ann N Y Acad Sci 1116:281–290

(9) Pittenger MF, Mackay AM, Beck SC, Jaiswal RK, Douglas R, Mosca JD, Moorman MA, Simonetti DW, Craig S, DR Marshak (1999) **Multilineage potential of adult human mesenchymal stem cells**. Science 284:143–147

(10) Bar-Shavit Z. **The osteoclast: a multinucleated, hematopoietic-origin, bone-resorbing osteoimmune cell**. Journal of Cellular Biochemistry. 2007; 102(5):1130–1139.

(11) Parfitt AM (1988) **Bone remodeling**. Henry Ford Hosp Med J 36:143–144

(12) Miyamoto, Takeshi. 2011. "**Regulators of Osteoclast Differentiation and Cell–Cell Fusion**." 101–5.

(13) Feng X. & McDonald J. M. **Disorders of bone remodeling**. Annual review of pathology 6, 121–145

(14) Xu F. & Teitelbaum S. L. **Osteoclasts: New Insights**. Bone Res 1, 11–26 (2013).

(15) Boyle W.J., Simonet W.S., Lacey D.L. **Osteoclast differentiation and activation**. Nature. 2003;423:337–342.

(16) Ikeda, Kyoji and Sunao Takeshita. 2015. "**The Role of Osteoclast Differentiation and Function in Skeletal Homeostasis**." Journal of Biochemistry 159(1):mvv112.

(17) Takahashi, Naoyuki, Nobuyuki Udagawa, and Tatsuo Suda. 2014. "**Vitamin D Endocrine System and Osteoclasts**." BoneKEy Reports 3(October 2013):1–9.

(18) NIH Consensus Development Panel on Osteoporosis Prevention, Diagnosis, and Therapy. **Osteoporosis prevention, diagnosis, and therapy**. JAMA. 2001;285:785–795.

(19) Seeliger, Claudine, Elizabeth R. Balmayor, and Martijn Van Griensven. 2016. "**miRNAs Related to Skeletal Diseases**." 00(00):1–21.

(20) Hernlund E, Svedbom A, Ivergård M, Compston J, Cooper C, Stenmark J, McCloskey EV, Jönsson B, Kanis JA. **Osteoporosis in the European Union: medical management, epidemiology and economic burden**. Arch Osteoporos. 2013;8(1-2):136.

(21) Ji, Xiao, Xiang Chen, and Xijie Yu. 2016. "**MicroRNAs in Osteoclastogenesis and Function: Potential Therapeutic Targets for Osteoporosis**." International Journal of Molecular Sciences 17(3):349.

(22) Rachner TD, S Khosla and LC Hofbauer. (2011). **Osteoporosis: now and the future**. Lancet 377:1276–1287.

(23) Kocijan R, Muschitz C, et al. **Circulating microRNA signatures in patients with idiopathic and postmenopausal osteoporosis and fragility fractures**. J Clin Endocrinol Metab. 2016 Aug 23.

(24) WHO Scientific Group on the **Assessment of Osteoporosis at Primary Health Care Level**. Summary Meeting Report. Geneva: World Health Organization; 2007.

(25) Aspray, T.J., 2015. **Fragility fracture: recent developments in risk assessment.** Ther. Adv. Musculoskelet. Dis. 7, 17–25.

(26) He L, Hannon GJ. **MicroRNAs: small RNAs with a big role in gene regulation**. Nat Rev Genet. 2004;5:522–531.

(27) Ji, Xiao, Xiang Chen, and Xijie Yu. 2016. "**MicroRNAs in Osteoclastogenesis and Function: Potential Therapeutic Targets for Osteoporosis**." International Journal of Molecular Sciences 17(3):349.

(28) Lee, R.C., Feinbaum, R.L. & Ambros, V., 1993. **The C. elegans heterochronic gene lin-4 encodes small RNAs with antisense complementarity to lin-14**. Cell, 75(5), pp.843–854.

(29) Kapinas, Kristina and Anne M. Delany. 2011. "**MicroRNA Biogenesis and Regulation of Bone Remodeling**." 8:1–11.

(30) Kim VN. **MicroRNA biogenesis: coordinated cropping and dicing**. Nat Rev Mol Cell Biol. 2005;6:376–385.

(31) Winter, J. et al., 2009. **Many roads to maturity: microRNA biogenesis pathways and their regulation**. Nature cell biology, 11, pp.228–234.

(32) Jing, Dian et al. 2015. "**The Role of microRNAs in Bone Remodeling**." (14):131–43.

(33) Mizoguchi F, Izu Y, Hayata T et al. **Osteoclast-specific Dicer gene deficiency suppresses osteoclastic bone resorption**. J Cell Biochem 2010; 109(5): 866–875.

(34) Sugatani T, Hruska KA (2009) **Impaired micro-RNA pathways diminish osteoclast differentiation and function.** J Biol Chem284:4667–4678.

(35) Sugatani T, Hildreth BE 3rd, Toribio RE et al. **Expression of DGCR8-dependent microRNAs is indispensable for osteoclastic development and bone-resorbing activity**. J Cell Biochem 2014; 115(6): 1043–1047.

(36) Moore B.T., Xiao P. **MiRNAs in bone diseases**. MicroRNA. 2013;2:20–31.

(37) Sugatani, T.; Vacher, J.; Hruska, K.A. **A microRNA expression signature of osteoclastogenesis**. Blood 2011,117, 3648–3657.

(38) Garcia Palacios, V.; Robinson, L.J.; Borysenko, C.W.; Lehmann, T.; Kalla, S.E.; Blair, H.C. **Negative regulation of RANKl-induced osteoclastic differentiation in raw264.7 cells by estrogen and phytoestrogens**. J. Biol.Chem. 2005, 280, 13720–13727.

(39) Sugatani, T.; Hruska, K.A. **Down-regulation of miR-21 biogenesis by estrogen action contributes to osteoclastic apoptosis**. J. Cell. Biochem. 2013, 114, 1217–1222.

(40) Cheng, P.; Chen, C.; He, H.B.; Hu, R.; Zhou, H.D.; Xie, H.; Zhu, W.; Dai, R.C.; Wu, X.P.; Liao, E.Y.; et al. **miR-148a regulates osteoclastogenesis by targeting v-maf**

musculoaponeurotic fibrosarcoma oncogene homolog b. J. Bone Miner. Res. 2013, 28, 1180–1190.

(41) Hackl, Matthias, Ursula Heilmeier, Sylvia Weilner, and Johannes Grillari. 2016. "**Molecular and Cellular Endocrinology Circulating microRNAs as Novel Biomarkers for Bone Diseases E Complex Signatures for Multifactorial Diseases ?**" Molecular and Cellular Endocrinology 432:83–95.

(42) Wang, Yang et al. 2012. "**MiR-133a in Human Circulating Monocytes : A Potential Biomarker Associated with Postmenopausal Osteoporosis**." 7(4):1–7.

(43) Seeliger, Claudine et al. 2014. "J BMR **Five Freely Circulating miRNAs and Bone Tissue miRNAs Are Associated With Osteoporotic Fractures**." 29(8):1718–28.

(44) Weilner S, et al. **Differentially circulating miRNAs after recent osteoporotic fractures can influence osteogenic differentiation**. Bone 2015; 79: 43-51.

(45) Heilmeier U, Hackl M, et al. **Serum microRNAs Are Indicative of Skeletal Fractures in Postmenopausal Women with and without Type 2 Diabetes and Influence Osteogenic and Adipogenic Differentiation of Adipose-Tissue Derived Mesenchymal Stem Cells In Vitro**. J Bone Miner Res 2016 Jun 27.

(46) Marino S, Logan JG, Mellis D, Capulli M. **Generation and culture of osteoclasts**. BoneKey Rep 2014; 3: 570.

(47) Collin-Osdoby P, Osdoby P. **RANKL-mediated osteoclast formation from murine RAW 264.7 cells**. Methods Mol Biol. 2012;816:187–202.

(48) Schmitz, Sabine. **Der Experimentator Zellkultur**, Spektrum Akademischer Verlag Heidelberg 2011 (3.Auflage)

(49) ATCC® **Animal Cell Culture Guide** 2014, www.atcc.org, (13.09.2016)

(50) Rahman, M. Motiur et al. 2015. "**Proliferation-Coupled Osteoclast Differentiation by RANKL : Cell Density as a Determinant of Osteoclast Formation**." Bone 81:392–99.

(51) Cuetara B. L. V., Crotti T. N., O'Donoghue A. J., McHugh K. P. **Cloning and characterization of osteoclast precursors from the RAW264.7 cell line**. In Vitro Cellular & Developmental Biology—Animal. 2006;42(7):182–188.

(52) Kim N, Takami M, Rho J, Josien R, Choi Y. **A novel member of the leukocyte receptor complex regulates osteoclast differentiation**. J Exp Med. 2002;195:201–209.

(53) Wu H, Xu G, Li YP. **Atp6v0d2 is an essential component of the osteoclast-specific proton pump that mediates extracellular acidification in bone resorption**. J Bone Miner Res. 2009;24:871–885.

(54) Xu, Juan, Feng Yue, Jingbo Wang, L. I. Chen, and Wenbo Qi. 2015. "**High Glucose Inhibits Receptor Activator of Nuclear Factor - κ B Ligand-Induced Osteoclast Differentiation via Downregulation of v - ATPase V0 Subunit d2 and Dendritic Cell - Specific Transmembrane Protein**." 1:865–70.

(55) Levaot, Noam et al. 2015. "**Osteoclast Fusion Is Initiated by a Small Subset of RANKL-Stimulated Monocyte Progenitors, Which Can Fuse to RANKL-Unstimulated Progenitors**." Bone 79:21–28.

(56) Hanahan D, Weinberg RA. **The hallmarks of cancer**. Cell. 2000;100:57–70.

(57) Kasagi, Shimpei and Wanjun Chen. 2013. "**TGF-beta1 on Osteoimmunology and the Bone Component Cells**." 1–7.

(58) Yasui T, Kadono Y, Nakamura M, Oshima Y, Matsumoto T, Masuda H, et al. **Regulation of RANKL-induced osteoclastogenesis by TGF-beta through molecular interaction between Smad3 and Traf6**. J Bone Miner Res. 2011;26(7):1447–56.

(59) Sells Galvin RJ, Gatlin CL, Horn JW, Fuson TR. **TGF-beta enhances osteoclast differentiation in hematopoietic cell cultures stimulated with RANKL and M-CSF**. Biochem Biophys Res Commun. 1999;265:233–239.

(60) Kaneda T, Nojima T, Nakagawa M, et al. **Endogenous production of TGF-beta is essential for osteoclastogenesis induced by a combination of receptor activator of NF-kappa B ligand and macrophage colony-stimulating factor**. J Immunol. 2000;165:4254–4263.

(61) Fuller, K., J. M. Lean, K. E. Bayley, M. R. Wani, and T. J. Chambers. 2000. "**A Role for TGF β 1 in Osteoclast Differentiation and Survival**." 2453:2445–53.

(62) Fox SW, Evans KE, Lovibond AC. **Transforming growth factor-beta enables NFATc1 expression during osteoclastogenesis**. Biochem Biophys Res Commun. 2008;366:123–128.

(63) Yan T, Riggs BL, Boyle WJ, Khosla S. **Regulation of osteoclastogenesis and RANK expression by TGF-beta1**. J Cell Biochem. 2001;83:320–325.

(64) Quinn J. M. W., Itoh K., Udagawa N., et al. **Transforming growth factor β affects osteoclast differentiation via direct and indirect actions**. Journal of Bone and Mineral Research. 2001;16(10):1787–1794.

(65) Karst M, Gorny G, Galvin RJ et al. **Roles of stromal cell RANKL, OPG, and M-CSF expression in biphasic TGF-beta regulation of osteoclast differentiation**. J Cell Physiol 2004; 200: 99–106.

(66) Zhang, H. et al. 2011. "**MiR-148a Promotes Apoptosis by Targeting Bcl-2 in Colorectal Cancer**." 1702–10.

15 Appendix

15.1 Melting curves

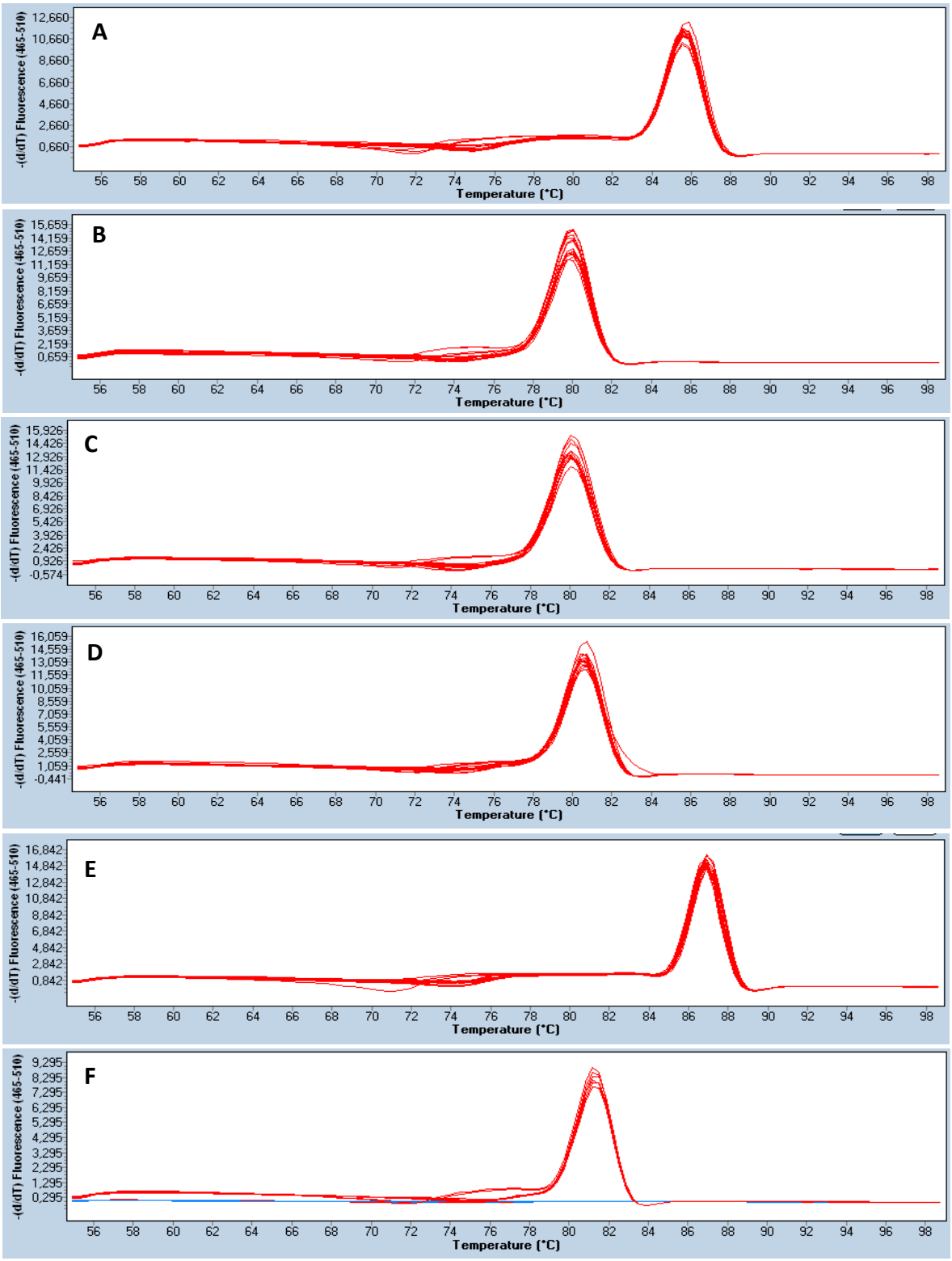

Figure 29: Melting curves.
(A) β-actin (B) Cathepsin K (C) TRAP (D) Atp6v0d2 (E) OSCAR (F) CalcR

15.2 Primer efficiency

Table 23: Primer efficiency

	β-actin	TRAP	Ctsk	Atp6v0d2	OSCAR	CalcR
Primer efficiency	**1.74**	**1.76**	**1.69**	**1.74**	**1.76**	**1.82**
Slope	-4.17	-4.08	-4.41	-4.15	-4.06	-3.85
Efficiency [%]	**86.80**	**87.88**	**84.32**	**87.04**	**88.19**	**90.93**